bioRxiv preprint doi: https://doi.org/10.1101/148429; this version posted March 30, 2018. The copyright holder for this preprint (which was not certified by peer review) is the author/funder, who has granted bioRxiv a license to display the preprint in perpetuity. It is made available under aCC-BY-NC-ND 4.0 International license.

Reciprocal Control of Motility and Biofilm Formation by the PdhS2 Two-Component Sensor Kinase of *Agrobacterium tumefaciens*

Jason E. Heindl[1,2], Daniel Crosby[2], Sukhdev Brar[2], Tiyan Singletary[2], Daniel Merenich[2], Justin L. Eagan[1], Aaron M. Buechlein[3], Eric L. Bruger[4], Christopher M. Waters[4] and Clay Fuqua[1*]

[1]Department of Biology
Indiana University
Bloomington, IN 47405, USA

[2]Department of Biological Sciences
University of the Sciences
Philadelphia, PA 19104, USA

[3]Center for Genomics and Bioinformatics
Indiana University
Bloomington, IN 47405

[4]Department of Microbiology and Molecular Genetics
Michigan State University
East Lansing, MI 48824, USA

bioRxiv preprint doi: https://doi.org/10.1101/148429; this version posted March 30, 2018. The copyright holder for this preprint (which was not certified by peer review) is the author/funder, who has granted bioRxiv a license to display the preprint in perpetuity. It is made available under aCC-BY-NC-ND 4.0 International license.

Running title: *Agrobacterium* PdhS2 regulates motility and biofilms

Keywords: Development, sensor kinase, phosphorelay, *Agrobacterium tumefaciens*, biofilm, motility

*Address for correspondence: Clay Fuqua, Dept. Biol., 1001 E. 3rd St., Jordan Hall 142, Indiana Univ., Bloomington, IN 47405-1847. Tel: 812-856-6005, FAX: 812-855-6705, E-mail: cfuqua@indiana.edu

Current addresses: J.E.H., Dept. Biol. Sci., Univ. Sci, Philadelphia, PA; E.L.B., Dept. Bio. Sci., Univ. Idaho, Moscow, ID 83844

Word count 9275 (without abstract, importance, acknowledgements, figure legends or references):

6 Figures, 2 Tables, 10 Supp. Figures, 3 Supp. Tables

bioRxiv preprint doi: https://doi.org/10.1101/148429; this version posted March 30, 2018. The copyright holder for this preprint (which was not certified by peer review) is the author/funder, who has granted bioRxiv a license to display the preprint in perpetuity. It is made available under aCC-BY-NC-ND 4.0 International license.

ABSTRACT

A core regulatory pathway that directs developmental transitions and cellular asymmetries in *Agrobacterium tumefaciens* involves two overlapping, integrated phosphorelays. One of these phosphorelays putatively includes four histidine sensor kinase homologues, DivJ, PleC, PdhS1, and PdhS2, and two response regulators, DivK and PleD. In several different alphaproteobacteria, this pathway influences a conserved downstream phosphorelay that ultimately controls the phosphorylation state of the CtrA master response regulator. The PdhS2 sensor kinase reciprocally regulates biofilm formation and swimming motility. In the current study the mechanisms by which the *A. tumefaciens* sensor kinase PdhS2 directs this regulation are delineated. PdhS2 lacking a key residue for phosphatase activity is markedly deficient in proper control of attachment and motility phenotypes, whereas a kinase-deficient PdhS2 mutant is only modestly affected. A genetic interaction between DivK and PdhS2 is revealed, unmasking one of several connections between PdhS2-dependent phenotypes and transcriptional control by CtrA. Epistasis experiments suggest that PdhS2 can function independently of the CckA sensor kinase, the cognate sensor kinase for CtrA which is inhibited by DivK. PdhS2 dynamically localizes to the daughter cell pole in dividing cells. Global expression analysis of the *pdhS2* mutant reveals a restricted regulon, functioning through CtrA to separately control motility and regulate levels of the intracellular signal cyclic diguanylate monophosphate (cdGMP), thereby affecting production of adhesive polysaccharides and attachment. We hypothesize that in *A. tumefaciens* the CtrA regulatory circuit has expanded to include additional inputs through addition of PdhS-

bioRxiv preprint doi: https://doi.org/10.1101/148429; this version posted March 30, 2018. The copyright holder for this preprint (which was not certified by peer review) is the author/funder, who has granted bioRxiv a license to display the preprint in perpetuity. It is made available under aCC-BY-NC-ND 4.0 International license.

type sensor kinases, likely fine-tuning the response of this organism to the soil microenvironment.

bioRxiv preprint doi: https://doi.org/10.1101/148429; this version posted March 30, 2018. The copyright holder for this preprint (which was not certified by peer review) is the author/funder, who has granted bioRxiv a license to display the preprint in perpetuity. It is made available under aCC-BY-NC-ND 4.0 International license.

63 **IMPORTANCE**

64 Bacterial developmental processes, such as morphological transformations and
65 behavioral transitions, are tightly regulated. In many alphaproteobacteria cell division
66 and development are coordinated by a specific suite of conserved histidine kinases and
67 their partnered regulatory proteins. Here we describe how the histidine kinase PdhS2 of
68 *Agrobacterium tumefaciens* regulates complex phenotypes including biofilm formation
69 and motility. PdhS2 genetically interacts with a single-domain response regulator, DivK,
70 and the intracellular signal cyclic diguanylate monophosphate. PdhS2 dynamically
71 localizes to the new pole of recently divided cells, contributing to the regulatory
72 processes that dictate whether these cells remain motile or initiate biofilm formation.
73 These findings expand our understanding of the complex network that integrates cell
74 division and developmental control in *A. tumefaciens* and related alphaproteobacteria.
75
76
77
78

bioRxiv preprint doi: https://doi.org/10.1101/148429; this version posted March 30, 2018. The copyright holder for this preprint (which was not certified by peer review) is the author/funder, who has granted bioRxiv a license to display the preprint in perpetuity. It is made available under aCC-BY-NC-ND 4.0 International license.

INTRODUCTION

Bacteria are sometimes considered to be elementary life forms, with simple body plans, streamlined reproductive cycles, and monolithic behavior when compared with higher eukaryotes. To the contrary, many bacteria can exhibit a remarkable diversity of developmental complexity, both temporal and morphological (1, 2). Even bacterial species whose cells appear morphologically uniform, such as rod-shaped *Escherichia coli* or coccoid *Staphylococcus aureus,* possess distinct cellular architectures as well as intricately timed cell division programs, and a large number of bacteria can form multicellular biofilms (3, 4). Developmental processes in bacteria, as in higher eukaryotes, are driven by factors that may be considered both cell-intrinsic and cell-extrinsic. Intrinsic factors include genomic and proteomic content, while extrinsic factors comprise environmental conditions, such as pH and temperature, which cells sense and to which they respond (5).

Members of the *Alphaproteobacteria* group include host-associated pathogens (*e.g. Brucella* sp., *Bartonella* sp.), host-associated commensals (*e.g. Sinorhizobium* sp., *Bradyrhizobium* sp.), and free-living aquatic and marine bacteria (*e.g. Caulobacter* sp., *Rhodobacter* sp., *Ruegeria* sp.). It is now recognized that several alphaproteobacteria divide asymmetrically, during which cells elongate, duplicate and segregate their genomic content between two non-equivalent compartments of predivisional cells, and finally generate two cells by cytokinesis (6, 7). Notably, cellular components are unevenly distributed between the two daughter cells during cell division, including surface structures (*e.g.* flagella and polar polysaccharides), cell wall components (*e.g.* peptidoglycan), and even cytoplasmic complexes (*e.g.* heat shock proteins). For

bioRxiv preprint doi: https://doi.org/10.1101/148429; this version posted March 30, 2018. The copyright holder for this preprint (which was not certified by peer review) is the author/funder, who has granted bioRxiv a license to display the preprint in perpetuity. It is made available under aCC-BY-NC-ND 4.0 International license.

example, there may be a clear segregation of existing organelles to one daughter cell while the second cell generates these structures *de novo* (6, 8-10). Although the specific details may vary among different taxa, the end result is the production of a young daughter cell and a comparatively aging mother cell. Not only does this uneven division partition senescence among the products of cell division, but it also allows for the generation of functionally distinct cell types. For example, in *Caulobacter crescentus* the non-motile stalked cell type can attach to surfaces using its polar adhesin called the holdfast (11). This stalked cell then serves as the mother cell during multiple rounds of cell division, generating and releasing motile swarmer cells upon each cytokinetic event (12). Motile swarmer cells are prohibited from entering the cell division cycle until differentiation into the non-motile stalked form (13, 14).

Underlying asymmetric cell division is subcellular differentiation that includes localization of specific regulatory proteins to programmed locations within each cell (15). Prominent among these in many alphaproteobacteria are components of two overlapping phosphorelays, the first which functions through the response regulators DivK and PleD (the DivK-PleD relay) and the second which functions primarily through the response regulator CtrA (the CtrA relay). The pathways are connected through DivK, which controls initiation of the CtrA relay by regulating its cognate sensor kinase CckA (16, 17). Collectively we refer to these two relays as the DivK-CtrA pathway. In the well-studied *C. crescentus* system the membrane-associated sensor histidine kinases PleC and DivJ control the phosphorylation state of DivK and PleD, and localize to opposing poles of the predivisional cell (18-21). Through antagonistic kinase and phosphatase activities on DivK and PleD, their target response regulators, PleC and

bioRxiv preprint doi: https://doi.org/10.1101/148429; this version posted March 30, 2018. The copyright holder for this preprint (which was not certified by peer review) is the author/funder, who has granted bioRxiv a license to display the preprint in perpetuity. It is made available under aCC-BY-NC-ND 4.0 International license.

DivJ inversely manifest their activity on the most downstream component of the DivK-CtrA pathway, the response regulator CtrA (22-25). DivJ is retained at the stalked cell pole and serves as a DivK/PleD kinase, increasing the DivK~P concentration and diminishing CtrA~P levels in this region of the cell (Fig. 1A). Conversely, PleC localizes to the pole distal to the stalk, where the single polar flagellum is assembled, dephosphorylating DivK, leading to increased CtrA~P levels and activity. Phospho-CtrA binds to the replication origin thereby preventing DNA replication, and also acts as a transcriptional regulator for many genes, including activating those for assembly of the flagellum and motility (26-28). The CtrA relay is also influenced by the DivK-PleD relay through levels of the second messenger cyclic diguanylate monophosphate (cdGMP). DivJ-dependent phosphorylation of PleD at the stalk pole of the predivisional cell stimulates its diguanylate cyclase activity, resulting in higher levels of cdGMP at this end of the cell. The CckA kinase that initiates the CtrA relay is also biased away from its kinase and towards its phosphatase activity by direct allosteric control through high levels of cdGMP, thereby reinforcing a CtrA~P gradient, relatively low at the stalk pole and increasing towards the distal pole (29-34) (Fig. 1A).

Agrobacterium tumefaciens is a plant pathogen of the *Alphaproteobacteria* class that is not stalked, but like *C. crescentus*, divides asymmetrically generating a motile daughter cell from a mother cell (6). As a facultative pathogen, the *A. tumefaciens* lifestyle substantially differs from that of the freshwater oligotroph *C. crescentus*. Nonetheless core components of the DivK-CtrA pathway are well conserved in *A. tumefaciens*, including three non-essential PleC/DivJ homologue sensor kinase (PdhS) homologues PleC (Atu0982), PdhS1 (Atu0614), and PdhS2 (Atu1888). The *divJ* gene

bioRxiv preprint doi: https://doi.org/10.1101/148429; this version posted March 30, 2018. The copyright holder for this preprint (which was not certified by peer review) is the author/funder, who has granted bioRxiv a license to display the preprint in perpetuity. It is made available under aCC-BY-NC-ND 4.0 International license.

(Atu0921) is essential in *A. tumefaciens* (35, 36). We have previously shown that the three non-essential PdhS homologues have distinct roles in the normal cellular development of *A. tumefaciens* (35). Mutants in PleC and PdhS1, as well as the *A. tumefaciens* DivK homologue, all manifested marked effects on cell division, with branched and elongated cells, as well as deficiencies in motility and biofilm formation. To date the essentiality of *divJ* has precluded exhaustive phenotypic analysis of its role (35). The fourth PdhS family member, PdhS2, does not appear to participate in regulation of cell division as all cells are morphologically wild-type in appearance (35). Loss of PdhS2, however, results in dramatically increased attachment and biofilm formation, and a simultaneous dramatic reduction in motility. Reciprocal regulation of these phenotypes is often a hallmark of regulation by cdGMP (37). In this work we further explore the mechanism by which PdhS2 regulates attachment and motility. Our results genetically connect DivK with PdhS2 and transcriptional profiling clearly implicates CtrA as their downstream regulatory effector. We also show a clear intersection of PdhS2 activity and the activity of several diguanylate cyclases, suggesting that PdhS2 and cdGMP coordinately regulate biofilm formation and motility in *A. tumefaciens*. Finally, we observe that PdhS2 dynamically localizes to the newly generated poles of both the new daughter cell and the mother cell following cytokinesis. Collectively, our findings suggest that PdhS2 activity is specifically required for proper development of motile daughter cells.

bioRxiv preprint doi: https://doi.org/10.1101/148429; this version posted March 30, 2018. The copyright holder for this preprint (which was not certified by peer review) is the author/funder, who has granted bioRxiv a license to display the preprint in perpetuity. It is made available under aCC-BY-NC-ND 4.0 International license.

RESULTS

Mutational analysis of PdhS2 reveals coordinate regulation through kinase and phosphatase activities. Members of the PdhS family of sensor histidine kinases contain a conserved HATPase_c catalytic domain at their carboxyl termini and an upstream conserved HisKA dimerization/phosphoacceptor domain. Many sensor kinases exhibit bifunctional catalytic activity, alternately acting as kinase or phosphatase, and *C. crescentus* PleC is one such example (18, 22, 38). Multiple sequence alignment of the HisKA domain from the *A. tumefaciens* and *C. crescentus* PdhS family kinase homologues reveals a high level of conservation of this domain including the phospho-accepting histidine residue (H271 of PdhS2) and a threonine residue predicted to be important for phosphatase activity (T275 of PdhS2) (Fig. 1B).

To test the requirement of the conserved phospho-accepting histidine for PdhS2 activity we mutated this residue to alanine (H271A). Ectopic expression of PdhS2^{H271A} (plasmid-borne P_{lac}-*pdhS2*, kinase-negative, K; phosphatase-positive, P$^+$) effectively complemented the attachment and motility phenotypes of the Δ*pdhS2* mutant similar to wild type *pdhS2* (Fig. 2A). These data indicate that this histidine residue is not crucial for PdhS2 regulation of swimming motility and biofilm formation. When *pdhS2* is ectopically expressed in the wild type, it causes a slight but significant stimulation of biofilm formation, and the *pdhS2*^{H271A} (K$^-$P$^+$) mutation reverses this effect.

Efficient phosphatase activity of many sensor kinases requires a conserved threonine residue roughly one α-helical turn (4 residues) downstream of the phospho-accepting histidine residue (39, 40). We therefore mutated this conserved threonine

bioRxiv preprint doi: https://doi.org/10.1101/148429; this version posted March 30, 2018. The copyright holder for this preprint (which was not certified by peer review) is the author/funder, who has granted bioRxiv a license to display the preprint in perpetuity. It is made available under aCC-BY-NC-ND 4.0 International license.

191 residue to alanine (Thr275A). In contrast to the PdhS2^{H271A} mutant protein (K^-P^+),
192 equivalent ectopic expression of the PdhS2^{T275A} allele (K^+P^-) failed to complement the
193 Δ*pdhS2* motility and attachment phenotypes, and in fact exacerbated them (Fig. 2A).
194 When expressed in wild type, the PdhS2^{T275A} allele (K^+P^-) caused modest stimulation of
195 biofilm formation and slightly decreased motility. A double mutant allele of PdhS2 with
196 both the histidine and threonine residues mutated (K^-P^-) had no effect on these
197 phenotypes (Fig. S1). Together these results suggest that it is the balance of kinase and
198 phosphatase activity that dictates PdhS2 control over its targets, with the kinase
199 stimulating biofilm formation and decreasing motility, and the phosphatase activity
200 diminishing biofilm formation and promoting motility. The phosphatase activity however,
201 appears to play the dominant role under laboratory culture conditions.
202
203 **Mutations in *divK* are epistatic to *pdhS2* mutations.** Members of the PdhS family of
204 sensor kinases were originally identified based on homology with their namesakes DivJ
205 and PleC of *C. crescentus* (41, 42) (Fig. 1B). Based on this homology all PdhS family
206 members are predicted to interact with the single domain response regulator DivK (42)
207 and also interact with the diguanylate cyclase response regulator PleD. Prior work from
208 our laboratory has shown that both swimming motility and adherent biomass are
209 diminished in the Δ*divK* mutant, implying that DivK activity is required for proper
210 regulation of these phenotypes in *A. tumefaciens* (35). In contrast, PdhS2 inversely
211 regulates these phenotypes; a Δ*pdhS2* mutant is non-motile but hyperadherent. To
212 determine whether PdhS2 genetically interacts with DivK we constructed a
213 Δ*divK*Δ*pdhS2* mutant and compared swimming motility and biofilm formation in this

bioRxiv preprint doi: https://doi.org/10.1101/148429; this version posted March 30, 2018. The copyright holder for this preprint (which was not certified by peer review) is the author/funder, who has granted bioRxiv a license to display the preprint in perpetuity. It is made available under aCC-BY-NC-ND 4.0 International license.

strain to wild-type and parental single deletion strains (Fig. 2B). As reported, loss of either *divK* or *pdhS2* reduced swimming motility as measured by swim ring diameter on motility agar. Biofilm formation on PVC coverslips in the Δ*divK* mutant was diminished relative to the wild-type C58 strain while for the Δ*pdhS2* mutant it was dramatically increased. The Δ*divK*Δ*pdhS2* mutant was similar to the Δ*divK* mutant in both assays, with no significant difference in the efficiency of either swimming motility or biofilm formation between the two strains. These data support the proposed genetic interaction between *divK* and *pdhS2*, with the *divK* mutation epistatic to *pdhS2* for biofilm formation and swimming motility.

Swim ring diameters of the Δ*divK* and Δ*divK*Δ*pdhS2* mutants were decreased by ~20% compared to wildtype whereas the decrease in Δ*pdhS2* swim ring diameters was ~40% compared to wildtype, suggesting that the nature of the defect in swimming motility differs between these two classes of mutants and that loss of *divK* partially restores motility in the absence of *pdhS2*. Indeed, it was earlier noted that although both the Δ*divK* and the Δ*pdhS2* single deletion mutants produce polar flagella, very few Δ*pdhS2* mutant bacteria were observed to be motile under wet-mount microscopy implying that the swimming defect is due to diminished flagellar activity rather than flagellar assembly (35). The Δ*divK* mutant, however, was readily observed to be motile under wet-mount microscopy. Similarly, the Δ*divK*Δ*pdhS2* mutant generates polar flagella and its motility is readily observed under wet-mount microscopy. Both the Δ*divK* and Δ*divK*Δ*pdhS2* mutants, and not the Δ*pdhS2* mutant, generate aberrant cell morphologies including elongated and branched cells (35) (Fig. S2).

bioRxiv preprint doi: https://doi.org/10.1101/148429; this version posted March 30, 2018. The copyright holder for this preprint (which was not certified by peer review) is the author/funder, who has granted bioRxiv a license to display the preprint in perpetuity. It is made available under aCC-BY-NC-ND 4.0 International license.

Further support for a genetic interaction between PdhS2 and DivK was provided by plasmid-borne, wild-type PdhS2 expressed ectopically from a P_{lac} promoter. Induced expression of *pdhS2* rescues swimming motility and returns biofilm formation closer to wild type levels in the Δ*pdhS2* mutant, albeit incompletely (Fig. 2A). However, as predicted from the Δ*divK*Δ*pdhS2* phenotypes, plasmid-borne provision of PdhS2 in the Δ*divK* mutant had no significant effect on either biofilm formation or swimming motility (Fig. 2C). Expression of either the kinase-null or the phosphatase-null allele of PdhS2 in the Δ*divK* background similarly had no effect on biofilm formation or swimming motility (Fig. 2C).

Kinase-locked allele of CckA does not suppress *pdhS2* phenotypes. One key PdhS target among multiple bacterial taxa is the hybrid histidine kinase CckA. CckA exhibits dynamic regulation dependent upon both phosphorylation status of DivK and local levels of cdGMP (31). CckA ultimately serves as either a source or a sink for CtrA phosphorylation through a phosphorelay that includes the histidine phosphotransferase ChpT (29). Previously we identified a mutation in CckA that results in a kinase-locked allele which is insensitive to regulation by DivK and cdGMP, $CckA^{Y674D}$ (31, 35). Expression of this allele in the Δ*pleC* background suppressed the swimming motility defect of the Δ*pleC* strain but had no effect on swimming motility in the Δ*divK* background (35). These results were consistent with PleC activity proceeding through DivK and with DivK negatively regulating CckA kinase activity. We reasoned that if PdhS2 similarly functioned through DivK and CckA, expression of $CckA^{Y674D}$ in the Δ*pdhS2* background would suppress the motility and biofilm phenotypes of this strain.

bioRxiv preprint doi: https://doi.org/10.1101/148429; this version posted March 30, 2018. The copyright holder for this preprint (which was not certified by peer review) is the author/funder, who has granted bioRxiv a license to display the preprint in perpetuity. It is made available under aCC-BY-NC-ND 4.0 International license.

259 However, induced expression of wild-type CckA or the CckA^{Y674D} allele only marginally
260 impacted these phenotypes (Fig. S3 and S4). These observations suggest that PdhS2
261 functions differently than PleC.
262
263 **PdhS2 and DivJ localize to the pole of *A. tumefaciens***. A mechanism for
264 establishing and maintaining developmental asymmetries in bacteria is the differential
265 polar localization of proteins with opposing functionalities (43, 44). Several members of
266 the PdhS family of sensor kinases localize to one or both bacterial poles (18, 22, 45).
267 Using a full-length PdhS2-GFP fusion that retains wild type functionality, expressed
268 from P_{lac} on a low copy number plasmid, we tracked localization of PdhS2 in *A.*
269 *tumefaciens* following IPTG induction (Fig. 3A). In both wild-type (data not shown) and
270 Δ*pdhS2* backgrounds PdhS2-GFP localized primarily to the new pole of predivisional
271 cells. Time-lapse microscopy of the Δ*pdhS2* mutant expressing PdhS2-GFP revealed
272 apparent dynamic relocalization of PdhS2-GFP to the newly generated pole of the
273 daughter cell coincident with cytokinesis. In the mother cell a new focus of PdhS2-GFP
274 subsequently accumulates at the new pole generated following septation and daughter
275 cell release. These time-lapse experiments clearly indicate that PdhS2-GFP localizes to
276 the actively growing pole of the cell, and is lost at that pole as it developmentally
277 matures and the cell proceeds to the predivisional state. Following cytokinesis PdhS2-
278 GFP localizes to the newly generated, younger poles of both the daughter cell and the
279 mother cell. This dynamic localization is consistent with PdhS2 activity being restricted
280 to the motile-cell compartment of predivisional cells and to newly generated motile cells.

bioRxiv preprint doi: https://doi.org/10.1101/148429; this version posted March 30, 2018. The copyright holder for this preprint (which was not certified by peer review) is the author/funder, who has granted bioRxiv a license to display the preprint in perpetuity. It is made available under aCC-BY-NC-ND 4.0 International license.

281 Since PdhS2 localizes to the new pole of dividing cells and primarily requires its
282 phosphatase activity there likely exist one or more old pole-localized kinases opposing
283 PdhS2 activity. The most obvious candidate for this is DivJ, which localizes to the old
284 pole in *C. crescentus* and acts as a DivK kinase in both *C. crescentus* and *S. meliloti*
285 (42, 46). Time-lapse microscopy of a full length DivJ-GFP fusion in wild-type *A.*
286 *tumefaciens* reveals localization to the old pole in mother cells that is not redistributed
287 over the course of multiple cell division cycles (Fig. 3B). Our findings are confirmed by a
288 recent report of similar localization patterns for PdhS2 and DivJ, which also
289 demonstrates PdhS1 localization to the old pole of the bacterium, similar to DivJ (47).
290
291 **Expression of predicted CtrA-dependent promoters.** The known architecture of the
292 DivK-CtrA pathway predicts that PdhS2 impacts developmental phenotypes through the
293 transcriptional regulator CtrA. In *C. crescentus*, CtrA is known to directly regulate at
294 least 55 operons, acting as either an activator or repressor of transcription, and to
295 control DNA replication (22, 28). *A. tumefaciens* CtrA is predicted to act similarly,
296 binding to DNA in a phosphorylation-dependent manner and regulating DNA replication
297 and transcription. *A. tumefaciens* CtrA is 84% identical to *C. crescentus* CtrA at the
298 amino acid level and purified *C. crescentus* CtrA binds to a site upstream of the *A.*
299 *tumefaciens ccrM* gene (48). Furthermore, computational analysis of multiple
300 alphaproteobacterial genomes uncovered numerous cell cycle regulated genes
301 preceded by a consensus CtrA binding site (49). We therefore evaluated CtrA activity by
302 examining the transcription of several known and predicted CtrA-dependent promoters
303 from both *C. crescentus* and *A. tumefaciens* in wild-type, Δ*pdhS2*, and Δ*divK A.*

bioRxiv preprint doi: https://doi.org/10.1101/148429; this version posted March 30, 2018. The copyright holder for this preprint (which was not certified by peer review) is the author/funder, who has granted bioRxiv a license to display the preprint in perpetuity. It is made available under aCC-BY-NC-ND 4.0 International license.

304 *tumefaciens* strain backgrounds. The *ccrM*, *ctrA*, and *pilA* promoters from *C. crescentus*
305 were chosen to represent CtrA-activated promoters likely to be similarly regulated in *A.*
306 *tumefaciens* (13, 14, 50, 51). In the Δ*pdhS2* background, expression levels from both
307 the *ctrA* and *pilA* promoters from *C. crescentus* were significantly reduced while
308 transcription from the *C. crescentus ccrM* promoter was unchanged (Table 1). In the *A.*
309 *tumefaciens* Δ*divK* background the *C. crescentus ccrM* and *ctrA* promoters exhibited
310 increased activity while the *pilA* promoter was unchanged (Table 1). These data are
311 consistent with *A. tumefaciens* CtrA regulating transcription of known CtrA-dependent
312 promoters, and with PdhS2 and DivK inversely regulating CtrA activity in *A.*
313 *tumefaciens*.

314 From *A. tumefaciens* the *ccrM* promoter is the only promoter for which prior
315 experimental data suggest CtrA-dependent regulation, thus this promoter was selected
316 for analysis (48). In addition to *ccrM*, putative *A. tumefaciens* promoters for *ctrA* and
317 *pdhS1* were selected for analysis based on the presence of at least one predicted CtrA
318 binding site as well as hypothesized cell cycle regulation of these loci. Transcriptional
319 activity from the *A. tumefaciens ctrA* and *pdhS1* promoter constructs showed inverse
320 regulation in the Δ*pdhS2* and Δ*divK* backgrounds, with expression decreased from the
321 *ctrA* promoter and increased for the *pdhS1* promoter in the Δ*pdhS2* mutant, and exactly
322 reversed in the Δ*divK* mutant. Although absence of *pdhS2* had little effect on the *A.*
323 *tumefaciens ccrM* promoter, transcription from this promoter was significantly increased
324 in the Δ*divK* background (Table 1). These data are congruent with the above data for *C.*
325 *crescentus* CtrA-dependent promoters and further support CtrA regulation of cell cycle-
326 responsive genes in *A. tumefaciens*.

bioRxiv preprint doi: https://doi.org/10.1101/148429; this version posted March 30, 2018. The copyright holder for this preprint (which was not certified by peer review) is the author/funder, who has granted bioRxiv a license to display the preprint in perpetuity. It is made available under aCC-BY-NC-ND 4.0 International license.

Global transcriptional analysis of PdhS2 activity. To determine the effect of PdhS2 activity on the *A. tumefaciens* transcriptome we used whole genome microarrays. Gene expression was compared between WT and Δ*pdhS2* strains grown to exponential phase in minimal media. Of 5338 unique loci represented on the arrays 39 genes were differentially regulated above our statistical cut-offs (P values, ≤ 0.05; $\log_2$ ratios of ≥ ± 0.50; Table 2). Of these, 24 genes were significantly upregulated, indicating negative regulation by PdhS2. Upregulated genes included *dgcB*, previously shown to contribute to elevated biofilm formation in hyperadherent *A. tumefaciens* mutants disrupted in the motility regulators VisN and VisR (52). Also upregulated was Atu3318, encoding a LuxR-type transcription factor, that similar to *dgcB* was previously identified by its elevated levels in *visNR* null mutants. Downregulated genes in the *pdhS2* mutant included six succinoglycan biosynthetic genes, consistent with our previous results showing positive regulation of succinoglycan production by PdhS2 (35).

To determine whether any of these 39 genes were putatively regulated by CtrA we scanned a sequence window from 500 bp upstream of the start codon to 100 bp into the coding sequence for plausible CtrA binding sites. CtrA binding sites were defined using the conserved alphaproteobacterial CtrA recognition sequence 5'-TTAANNNNNNGTTAAC-3' (48, 49). Sequences containing seven or more of the conserved nucleotides in this motif were deemed plausible candidates. Using these parameters 15 differentially transcribed loci are expressed from promoters (some from upstream genes in the operon) with putative CtrA binding sites and are thus putatively directly regulated by CtrA, including *dgcB* and Atu3318, as well as all five of the

bioRxiv preprint doi: https://doi.org/10.1101/148429; this version posted March 30, 2018. The copyright holder for this preprint (which was not certified by peer review) is the author/funder, who has granted bioRxiv a license to display the preprint in perpetuity. It is made available under aCC-BY-NC-ND 4.0 International license.

downregulated succinoglycan biosynthetic genes (Fig. S5; Table 2). We also identified numerous CtrA half-sites containing the sequence 5'-TTAA-3'. In *C. crescentus* CtrA has been shown to bind to such half motifs resulting in transcriptional effects (53). Twenty-eight promoters contained at least one CtrA half-site (Table 2).

To extend our microarray results we measured transcription of translational fusions to β-galactosidase for *dgcB* and Atu3318, in wild-type, Δ*pdhS2*, and Δ*divK* strain backgrounds (Table 1). In both cases β-galactosidase activity increased in the Δ*pdhS2* mutant, corroborating the microarray results. Furthermore, activity decreased from each promoter fusion in the Δ*divK* background supporting inverse regulation by PdhS2 and DivK at these promoters. Finally, to confirm a role for CtrA in transcriptional regulation by PdhS2 and DivK we mutated one CtrA half-site (-126 from start codon, TTAA to AATT) in the *dgcB* promoter region and evaluated transcription from this promoter fused to β-galactosidase as above. Surprisingly, activity from this mutated promoter was diminished in all backgrounds tested (wild-type, Δ*pdhS2*, and Δ*divK*) suggesting that CtrA does interact with this site to influence transcription of *dgcB*, but that this regulation is complex (Table 1). Overall these results are consistent with PdhS2 impacting the motile cell developmental program through CtrA-dependent transcriptional control.

Evaluation of CtrA protein levels. Turnover of CtrA is known to play a role in its regulatory activity in several related systems. To determine the effect of PdhS2 and DivK on CtrA activity and stability in *A. tumefaciens* we evaluated its steady-state levels and turnover in unsynchronized, stationary phase cultures using western blotting with antibodies raised against *C. crescentus* CtrA. In stationary phase cultures CtrA levels

bioRxiv preprint doi: https://doi.org/10.1101/148429; this version posted March 30, 2018. The copyright holder for this preprint (which was not certified by peer review) is the author/funder, who has granted bioRxiv a license to display the preprint in perpetuity. It is made available under aCC-BY-NC-ND 4.0 International license.

were increased in the Δ*pdhS2* background and decreased in the Δ*divK* background, but these effects were quite modest. This observation is however consistent with PdhS2 and DivK inversely impacting CtrA accumulation or stability (Fig. 4A).

CtrA protein stability was evaluated following treatment of wild-type and Δ*pdhS2* cultures with chloramphenicol to inhibit translation during exponential growth. In wild-type cultures, translation inhibition leads to a decline in CtrA abundance over the course of 2-3 hours, diminishing to roughly 30% of the steady-state levels. Loss of *pdhS2* had no effect on either final steady-state levels of CtrA following inhibition of translation or the observed rate of turnover when compared with wild-type cultures under these conditions (Fig. 4B).

PdhS2 activity intersects with cyclic-di-GMP pools. In *C. crescentus* DivJ and PleC positively regulate, via phosphorylation, a second response regulator, PleD, as well as DivK (22). In *C. crescentus* and *A. tumefaciens* the *divK* and *pleD* coding sequences form one operon and transcriptional regulation of both genes is linked. Since several PdhS kinases in these systems are predicted to interact with both DivK and PleD we analyzed the effect of loss of PleD activity in the Δ*pdhS2* background. As reported previously, deletion of *A. tumefaciens pleD* alone has only modest effects on swimming motility and adherent biomass (35). Loss of *pleD* in the Δ*pdhS2* background had a minimal effect on swimming motility (Fig. S6). Biofilm formation, however, was reduced by approximately 30%, indicating that PleD contributes to the increased attachment phenotype of the Δ*pdhS2* mutant (Fig. 5A).

bioRxiv preprint doi: https://doi.org/10.1101/148429; this version posted March 30, 2018. The copyright holder for this preprint (which was not certified by peer review) is the author/funder, who has granted bioRxiv a license to display the preprint in perpetuity. It is made available under aCC-BY-NC-ND 4.0 International license.

PleD is a GGDEF motif-containing diguanylate cyclase (DGC), and thus it is likely that the attachment phenotype of the Δ*pdhS2* mutant requires increased levels of cdGMP. Earlier work from our lab identified three additional DGCs that are relevant to attachment and biofilm formation: DgcA, DgcB, and DgcC (52). As seen in wild-type C58, deletion of *dgcA* or *dgcB* in the Δ*pdhS2* background significantly decreased attachment and biofilm formation, whereas loss of *dgcC* did not (Fig. 5A). These data suggest that increased biofilm formation by the Δ*pdhS2* mutant is dependent on cdGMP pools, generated through PleD, DgcA, or DgcB. Loss of *dgcB* largely abolishes the increased biofilm formation of the Δ*pdhS2* mutant. We also compared biofilm formation in Δ*dgcB*Δ*pleD* and Δ*pdhS2*Δ*dgcB*Δ*pleD* mutant backgrounds. In the absence of both DgcB and PleD biofilm formation was enhanced by loss of PdhS2 (Fig. S7). These data suggest that the increased biofilm formation of a *pdhS2* mutant is dependent on a cdGMP pool that is predominantly due to DgcB, but that is also under the cumulative influence of multiple DGC enzymes. Swimming motility was equivalent in either wild-type C58 or Δ*pdhS2* backgrounds in combination with mutations in *pleD*, *dgcA*, *dgcB*, or *dgcC* (Fig. S6 and S7).

Previously we found that mutants lacking either *dgcA*, *dgcB*, or *dgcC* show insignificant differences in total cytoplasmic levels of cdGMP (52). Nonetheless, loss of either *dgcA* or *dgcB*, or mutation of the GGDEF catalytic site of either enzyme, significantly reduced biofilm formation (52), implicating these enzymes in controlling the pool of cdGMP and thereby affecting attachment. We compared cytoplasmic cdGMP levels for wild-type C58, the Δ*pdhS2* mutant, and the Δ*pdhS2*Δ*dgcB* mutant strain and found these levels to be low, with no significant change between mutants (Fig. S8). To

bioRxiv preprint doi: https://doi.org/10.1101/148429; this version posted March 30, 2018. The copyright holder for this preprint (which was not certified by peer review) is the author/funder, who has granted bioRxiv a license to display the preprint in perpetuity. It is made available under aCC-BY-NC-ND 4.0 International license.

verify that the DGC activity is responsible for the increased biofilm formation in the Δ*pdhS2* background we expressed an allele of *dgcB* with a mutation in its GGDEF catalytic motif (GGAAF; *dgcB**) that abrogates cdGMP formation and that fails to complement a Δ*dgcB* mutant for either cdGMP formation or attachment phenotypes (52). Plasmid-borne expression of wild-type *dgcB* (P_{lac}-*dgcB*) results in a massive increase in attachment and biofilm formation in either the wild-type C58 or Δ*pdhS2* background (Fig. 5B). Expression of *dgcB** from a P_{lac} promoter, however, did not increase biofilm formation in either background. In the Δ*pdhS2*Δ*dgcB* mutant background expression of wild-type *dgcB* increased biofilm formation to the same degree seen in the wild-type and Δ*pdhS2* mutant. Expression of the mutant *dgcB** allele in the Δ*pdhS2*Δ*dgcB* mutant did appear to modestly affect biofilm formation, although far less than with the wild-type *dgcB* allele. Swimming motility was modestly but significantly reduced when the wild-type *dgcB* allele was provided *in trans* and this was abolished by the *dgcB** mutation (Fig. S9). Together our data are consistent with PdhS2-dependent biofilm formation and, to a lesser extent, swimming motility, being mediated at least in part by cdGMP levels.

Increased attachment in a *pdhS2* mutant requires the UPP polysaccharide. We have previously reported that PleD-stimulated attachment was due to increased levels of the unipolar polysaccharide (UPP) and cellulose (52). In addition to UPP and cellulose, *A. tumefaciens* produces at least three other exopolysaccharides: succinoglycan, cyclic β-1, 2 glucans, β-1, 3 glucan (curdlan), as well as outer membrane associated lipopolysaccharide (LPS) (54). Of these only LPS is essential for *A.*

bioRxiv preprint doi: https://doi.org/10.1101/148429; this version posted March 30, 2018. The copyright holder for this preprint (which was not certified by peer review) is the author/funder, who has granted bioRxiv a license to display the preprint in perpetuity. It is made available under aCC-BY-NC-ND 4.0 International license.

441 *tumefaciens* growth (36). The Δ*pdhS2* strain was tested for the impact of each of the
442 non-essential exopolysaccharides for biofilm formation and swimming motility. The *upp*
443 mutation completely abolished attachment in both the wild type and the *pdhS2* mutant
444 (Fig. S10A). The *chvAB* mutant, known to have pleiotropic effects (55), was diminished
445 in adherence overall, but was still elevated by the *pdhS2* mutation. None of the other
446 exopolysaccharide pathways impacted adherence in either background. The decreased
447 swimming phenotype of the *pdhS2* mutant was not significantly altered for any of the
448 exopolysaccharide mutants (Fig. S10B). These results indicate that biofilm formation in
449 the Δ*pdhS2* strain is dependent primarily on UPP production and that the motility
450 phenotype of the Δ*pdhS2* mutant is not dependent on any of the known
451 exopolysaccharides.
452
453

bioRxiv preprint doi: https://doi.org/10.1101/148429; this version posted March 30, 2018. The copyright holder for this preprint (which was not certified by peer review) is the author/funder, who has granted bioRxiv a license to display the preprint in perpetuity. It is made available under aCC-BY-NC-ND 4.0 International license.

DISCUSSION

PdhS2 regulates attachment and motility predominantly by its phosphatase activity and through CtrA. Regulation of the developmental program of many alphaproteobacteria centers on the global transcriptional regulator CtrA (43, 49, 56, 57). CtrA activity is controlled, indirectly, through a series of phosphotransfer reactions dependent on one or more PdhS-type histidine kinases. Here we show that PdhS2, one of at least four PdhS family kinases from *A. tumefaciens*, regulates motility and attachment at least in part through fine-tuning of CtrA activity, thereby impacting the CtrA regulon. We demonstrate that null mutations of the single domain response regulator *divK* are epistatic to *pdhS2* mutations in *A. tumefaciens*. Mutation of specific DGCs also reverse the phenotypes of *pdhS2* mutants, suggesting that elevated attachment and decreased motility are mediated through cdGMP pools. The phosphatase activity of PdhS2 is predominantly responsible for its function during laboratory culture growth. It is worth noting however, that strains bearing the phosphatase-null and kinase-null alleles of PdhS2 do not phenocopy one another nor the Δ*pdhS2* mutant strains, supporting distinct roles for both enzymatic activities. This is in contrast to mutant alleles of *pleC* in *C. crescentus* (46, 58, 59). Fine-scale determination of the timing, specificity, and regulation of both phosphatase and kinase activities await further experimentation.

Indirect regulation of CtrA by PdhS2. Our data support altered CtrA activity as responsible for many of the *pdhS2*-dependent transcriptional responses, and through these motility and attachment. A significant fraction of the differentially expressed genes had presumptive CtrA binding sites in their upstream regions. Several of the genes

bioRxiv preprint doi: https://doi.org/10.1101/148429; this version posted March 30, 2018. The copyright holder for this preprint (which was not certified by peer review) is the author/funder, who has granted bioRxiv a license to display the preprint in perpetuity. It is made available under aCC-BY-NC-ND 4.0 International license.

478 examined directly were dysregulated in both *pdhS2* and *divK* mutants, but usually in the
479 opposite directions. We predict that both DivK and PdhS2 function through affecting the
480 phosphorylation state of CtrA. In *A. tumefaciens* CtrA activates certain promoters (*e.g.*
481 succinoglycan synthetic genes and *ctrA*) while repressing others (*e.g. dgcB*, Atu3318,
482 and *pdhS1*). Although the *pdhS2* and *divK* mutations do slightly change steady state
483 levels of CtrA, our findings suggest that changes in CtrA stability do not explain the
484 resulting phenotypes. We posit that the phosphorylation state of CtrA is the dominant
485 mechanism by which its activity is affected in these mutants. There are several
486 examples in *C. crescentus* where altered CtrA activity is observed without significant
487 changes in CtrA abundance (36, 60, 61). There are also several examples in both *C.*
488 *crescentus* and *S. meliloti* where altered PdhS kinase activity results in both perturbed
489 activity and altered abundance of CtrA (42, 62). The subtle effects on CtrA abundance
490 coupled with the modest, but significant, effects we observed for several CtrA-
491 dependent promoters, suggest that PdhS2 regulation of CtrA activity may be restricted
492 to a very tight window during the cell cycle. Alternatively, the complement of remaining
493 PdhS kinases may buffer CtrA activity in the absence of *pdhS2*.
494
495 **PdhS2 influences cdGMP-dependent phenotypes.** The increased biofilm formation
496 and diminished motility in a *pdhS2* mutant is most similar to the inverse regulation
497 frequently observed for increasing internal pools of cdGMP (63). Indeed, our data
498 demonstrate a strong dependence on specific diguanylate cyclases for mediating the
499 Δ*pdhS2* hyperadherent phenotype, and transcription analysis demonstrates that *dgcB*
500 expression is elevated in this mutant. Although measurements of the cytoplasmic

bioRxiv preprint doi: https://doi.org/10.1101/148429; this version posted March 30, 2018. The copyright holder for this preprint (which was not certified by peer review) is the author/funder, who has granted bioRxiv a license to display the preprint in perpetuity. It is made available under aCC-BY-NC-ND 4.0 International license.

cdGMP levels suggest that they remain low overall in the *pdhS2* mutant, it is clear that mutations in *dgcB* strongly reverse the effects of the *pdhS2* mutation on attachment and that, to a lesser extent, mutations in *dgcA* and *pleD* can diminish them. This suggests that increased cdGMP synthesis via these enzymes may impart the effect on UPP-dependent attachment. Although DgcB seems to have the dominant effect, it is plausible that PdhS2 may affect PleD DGC activity through the phosphorylation state of its receiver domain, similar to other PleD homologues (22, 64, 65). In *A. tumefaciens* PleD has only modest effects on motility and attachment, and does not significantly contribute to cell cycle control (35). Neither DgcB nor DgcA is a response regulator, and it is more likely that at least for *dgcB,* its elevated expression is the mechanism through which CtrA functions. Recent studies have revealed that the *C. crescentus* orthologue of *A. tumefaciens* DgcB regulates holdfast synthesis in response to changes in flagellar rotation (66). Thus, changes in *dgcB* levels due to mutation of *pdhS2* may be also be impacting the motile to sessile transition in *A. tumefaciens*.

The phenotypes regulated by PdhS2 mirror those regulated by the master motility regulators VisR and VisN (52). Loss of either *visN* or *visR* results in abolishment of motility and a dramatic increase in attachment that is dependent on cdGMP production and the UPP adhesin. However, the motility defect in *visNR* mutants is predominantly transcriptional, as expression of all of the flagellar genes is dramatically decreased. In contrast, none of the flagellar genes are differentially regulated in the *pdhS2* mutant as measured in our microarray data, and flagella are assembled but decreased in activity. The increased attachment in *visNR* mutants is however due to elevated *dgcB* expression and also requires *dgcA*, through increased cdGMP and

bioRxiv preprint doi: https://doi.org/10.1101/148429; this version posted March 30, 2018. The copyright holder for this preprint (which was not certified by peer review) is the author/funder, who has granted bioRxiv a license to display the preprint in perpetuity. It is made available under aCC-BY-NC-ND 4.0 International license.

524 elevation of UPP and cellulose biosynthesis (52). Interestingly, other target genes that
525 are derepressed in *pdhS2* mutants are also among the small fraction of the genes that
526 are increased in a *visR* mutant, such as Atu3188. Given the presence of CtrA boxes in
527 their upstream sequences this may suggest a common underlying mechanism.
528 Interestingly, mutation of *dgcB* or the other DGCs does not enhance the dramatically
529 impeded motility of the *pdhS2* mutant. This suggests that the loss of motility in the
530 *pdhS2* mutant is not primarily due to elevated cdGMP levels. In many systems, CtrA
531 directly regulates motility, often through flagellar gene expression (67, 68). In fact,
532 plasmid-borne expression of the *A. tumefaciens* CtrA in a *ctrA* null mutant of the marine
533 alphaproteobacterium *Ruegeria* sp. KLH11 (*ctrA* is not essential in this taxon),
534 effectively reverses its non-motile phenotype (69), indicative of its positive impact on
535 motility on this bacterium. It seems likely that the non-motile phenotype of the *A.*
536 *tumefaciens pdhS2* mutant likewise reflects a decrease in active CtrA.
537 Interestingly, as shown for *C. crescentus* and *A. tumefaciens*, elevated cdGMP
538 allosterically switches the bifunctional hybrid histidine kinase CckA from kinase to
539 phosphatase mode, thereby downregulating CtrA phosphorylation and DNA-binding
540 activity (30, 31). Thus effects on local cdGMP levels can feed back on the CtrA
541 pathway, reinforcing decreases in CtrA~P that would be coincident with increased
542 cdGMP.
543
544 **Segregation of antagonistic signaling activity promotes asymmetric development.**
545 The asymmetric division of *A. tumefaciens* and other alphaproteobacteria, producing
546 two genetically identical but phenotypically distinct daughter cells, requires well-

bioRxiv preprint doi: https://doi.org/10.1101/148429; this version posted March 30, 2018. The copyright holder for this preprint (which was not certified by peer review) is the author/funder, who has granted bioRxiv a license to display the preprint in perpetuity. It is made available under aCC-BY-NC-ND 4.0 International license.

547 coordinated regulation of two developmental programs. The mother cell remains in a
548 terminally differentiated state, proceeding through distinct synthesis (S) and growth
549 (G1/G2) phases of the cell cycle (54, 56). During G1/G2 phase the cell elongates into a
550 predivisional cell and establishes a functional asymmetry between its two cellular poles
551 by differential localization of antagonistic homologues of the PdhS kinases. At least one
552 PdhS kinase localizes to the old pole; DivJ in *C. crescentus*, DivJ and PdhS1 in *A.*
553 *tumefaciens* (Fig. 1A and 3B), PdhS in *B. abortus*, and CbrA in *S. meliloti*, (18, 41, 47).
554 From this position these kinases can act to phosphorylate targets such as DivK and
555 PleD, indirectly inactivating CtrA (as reported for *C. crescentus*). At the opposite pole at
556 least one PdhS kinase, PleC in *C. crescentus* and PdhS2 in *A. tumefaciens* (Fig. 1A
557 and 3A), localizes and acts primarily through its phosphatase activity to
558 dephosphorylate targets, ultimately promoting CtrA stability and activity. Upon
559 cytokinesis, then, the motile daughter cell is released in a G1/G2 growth phase with
560 high levels of CtrA activity establishing a distinct transcriptional program and limiting
561 DNA replication.

562 Our data are consistent with PdhS2 acting in the motile daughter cell to prevent
563 premature activation of cell attachment processes, as well as to promote motility. PdhS2
564 dynamically localizes to the new pole of *A. tumefaciens* cells following cytokinesis while
565 DivJ, another PdhS-type kinase, localizes to the old pole of each cell. We propose that
566 together the antagonistic activities of DivJ and PdhS2 (and perhaps additional PdhS
567 homologues), coupled with their distinct localization patterns, generate a spatiotemporal
568 gradient of phospho-CtrA, thus differentially regulating the developmental program of *A.*
569 *tumefaciens* (Fig. 1A). Localized synthesis and degradation of cdGMP contributes to

bioRxiv preprint doi: https://doi.org/10.1101/148429; this version posted March 30, 2018. The copyright holder for this preprint (which was not certified by peer review) is the author/funder, who has granted bioRxiv a license to display the preprint in perpetuity. It is made available under aCC-BY-NC-ND 4.0 International license.

570 this regulatory gradient. Prior to and after cytokinesis daughter cells would have PdhS2
571 at their flagellar pole, reinforcing the CtrA pathway, increasing CtrA~P, promoting
572 motility and preventing adhesive processes. In contrast, at the mother cell old pole after
573 PdhS2 delocalization, DivJ kinase activity would dominate, the CtrA pathway would be
574 inhibited, and lower CtrA~P levels would promote DNA replication, maintaining a
575 sessile, non-motile state. Computational models of asymmetric cell development in *C.*
576 *crescentus* support this notion, with the important *caveat* that phospho-DivK may not be
577 distributed in a gradient but rather locally restricted (23, 25, 70).
578
579 **PdhS2 may regulate CtrA activity via an alternate route.** The recognized
580 architecture of the DivK-CtrA regulatory pathway in several alphaproteobacteria,
581 coupled with our data demonstrating a genetic interaction between *divK* and *pdhS2* in
582 *A. tumefaciens*, are consistent with PdhS2, primarily through its phosphatase activity,
583 decreasing DivK phosphorylation, similar to what is predicted for the other PdhS-type
584 kinase PleC (Fig. 6, Model A). The *pdhS2* mutant phenotype is however in stark
585 contrast to the other non-essential *A. tumefaciens* PdhS-type mutants and the *divK*
586 mutant, which all cause cell branching (35). How does PdhS2 regulate the same
587 pathway so differently from the PdhS-type proteins? Possibly, spatial restriction of
588 PdhS2 activity to the new poles of mother cells, that rapidly transition to become the old
589 pole of newly formed daughter cells, imparts PdhS2 control of motility and attachment
590 processes, without strongly influencing the budding process *per se.* Alternatively,
591 PdhS2 may act via a different mechanism to influence CtrA activity.

bioRxiv preprint doi: https://doi.org/10.1101/148429; this version posted March 30, 2018. The copyright holder for this preprint (which was not certified by peer review) is the author/funder, who has granted bioRxiv a license to display the preprint in perpetuity. It is made available under aCC-BY-NC-ND 4.0 International license.

592 An interesting possibility is that PdhS2 and DivK may work in parallel rather than
593 in series to impact CtrA activity and its target genes (Fig. 6, Model B). The apparent
594 epistasis of the *divK* mutation over the *pdhS2* mutation could result from the unfettered
595 activity of CckA in the *divK* mutant, which titrates the impact of the *pdhS2* mutation. Our
596 results in which expression of wild-type and kinase-locked CckA ($CckA^{Y67D}$) alleles in
597 the Δ*pdhS2* mutant only modestly impact its mutant phenotypes, support this proposal
598 (Fig. S3 and S4). The $CckA^{Y67D}$ mutant was isolated as a spontaneous suppressor of
599 the swimming deficiency of a *pleC* mutant (35). Plasmid-borne ectopic expression of the
600 $CckA^{Y67D}$ effectively reversed *pleC* phenotypes, in contrast to the observation that it
601 does not suppress *pdhS2* mutant phenotypes (Fig. S3 and S4). This suggests that
602 PdhS2 does not act similarly to PleC to inhibit DivK phosphorylation. A plausible
603 explanation is that PdhS2 control of CtrA activity is independent of DivK and CckA (Fig.
604 6, Model B). Although uninhibited CckA kinase activity in a *divK* mutant can overcome
605 the effect of the *pdhS2* mutation, perhaps the kinase-locked $CckA^{Y67D}$ allele is
606 insufficiently active to do so.

607 In this model, PdhS2 intercepts the DivK-CtrA signaling axis at a node
608 downstream or independent of CckA (Fig. 6). Our findings reveal that the phosphatase
609 activity of PdhS2 is dominant in its impact on CtrA-dependent targets, suggesting that it
610 dephosphorylates a response regulator that itself is inhibitory to CtrA activity. A
611 response regulator that inhibits CtrA directly is CpdR (Fig. 6), which in *C. crescentus*
612 stimulates proteolytic turnover of CtrA (71). *A. tumefaciens* has two CpdR homologues,
613 CpdR1 and CpdR2 (Atu3883 and Atu3603, respectively). *S. meliloti* likewise maintains
614 two CpdR homologues one of which, CpdR1, impacts developmental phenotypes and

bioRxiv preprint doi: https://doi.org/10.1101/148429; this version posted March 30, 2018. The copyright holder for this preprint (which was not certified by peer review) is the author/funder, who has granted bioRxiv a license to display the preprint in perpetuity. It is made available under aCC-BY-NC-ND 4.0 International license.

615 CtrA activity (62, 72). However, current models suggest that for CpdR in *C. crescentus*
616 and CpdR1 in *S. meliloti*, phosphorylation through ChpT decreases its ability to drive
617 CtrA degradation. Therefore, in *A. tumefaciens*, if PdhS2 acts on the pathway through
618 its phosphatase activity, dephosphorylation of CpdR1 would increase its inhibitory
619 capacity for CtrA. Mutation of *pdhS2* would then be predicted to lead to more CtrA~P
620 available to inhibit *dgcB* expression and stimulate motility, generating the opposite of
621 the non-motile, hyperadherent phenotypes we observe. It is formally possible that in *A.*
622 *tumefaciens* CpdR functions differently than its orthologues in *C. crescentus* or *S.*
623 *meliloti,* or that the PdhS2 target is a different response regulator.
624 A plausible alternative target for PdhS2 is CpdR2 (Atu3603). The CpdR2
625 response regulator of *S. meliloti* does not impact developmental phenotypes (77),
626 consistent with our own observations for *cpdR2* mutants of *A. tumefaciens* (Heindl et al.
627 unpublished results). If not CpdR2, the target could be a response regulator (RR-X) that
628 is thus far unrecognized to function in CtrA control (Fig. 6). In either case, one would
629 predict that the phosphorylated form of the response regulator is active for CtrA
630 inhibition, and that dephosphorylation by PdhS2 diminishes its inhibitory activity on
631 CtrA. Conversely, *pdhS2* mutants promote the strongly activated form of this response
632 regulator, inhibiting CtrA, derepressing *dgcB* expression and limiting motility, and in turn
633 driving cdGMP-responsive attachment. We have previously proposed additional direct
634 targets for the PdhS-type kinase DivJ as a means to explain the contradiction between
635 the essentiality of *divJ* and the non-essentiality of *divK* in *A. tumefaciens* (35). In that
636 work we also noted the possibility of DivJ directly targeting CtrA as observed *in vitro* for
637 *C. crescentus* DivJ. It is thus possible that both DivJ and PdhS2 in *A. tumefaciens* act

bioRxiv preprint doi: https://doi.org/10.1101/148429; this version posted March 30, 2018. The copyright holder for this preprint (which was not certified by peer review) is the author/funder, who has granted bioRxiv a license to display the preprint in perpetuity. It is made available under aCC-BY-NC-ND 4.0 International license.

638 downstream of CckA, perhaps both through RR-X (Fig. 6), more directly influencing
639 CtrA (73).These models are currently being tested, but are more challenging due to the
640 essentiality of many of the regulatory components in this domain of the pathway for *A.*
641 *tumefaciens*, including DivJ itself.
642

bioRxiv preprint doi: https://doi.org/10.1101/148429; this version posted March 30, 2018. The copyright holder for this preprint (which was not certified by peer review) is the author/funder, who has granted bioRxiv a license to display the preprint in perpetuity. It is made available under aCC-BY-NC-ND 4.0 International license.

643 ## MATERIALS AND METHODS

644

645 **Strains and plasmids.** Bacterial strains, plasmids, and oligonucleotides used in these
646 studies are listed in Tables S1 through S3. *A. tumefaciens* was routinely cultivated at
647 28°C in AT minimal medium plus 1% (w/v) glucose as a carbon source and 15 mM
648 $(NH_4)_2SO_4$ as a nitrogen source (ATGN), without exogenous $FeSO_4$ (74, 75). For biofilm
649 assays 22 μM $FeSO_4$ was included in the media. *E. coli* was routinely cultivated at 37°C
650 in lysogeny broth (LB). Antibiotics were used at the following concentrations (*A.*
651 *tumefaciens*/*E. coli*): ampicillin (100/100 $\mu g \cdot mL^{-1}$), kanamycin (150/25 $\mu g \cdot mL^{-1}$),
652 gentamicin (150/30 $\mu g \cdot mL^{-1}$), spectinomycin (300/100 $\mu g \cdot mL^{-1}$), and tetracycline (4/10
653 $\mu g \cdot mL^{-1}$).

654 Non-polar, markerless deletion of *pdhS2* (Atu1888) in all genetic backgrounds
655 used in this work was accomplished using splicing by overlap extension (SOE)
656 polymerase chain reaction (PCR) followed by homologous recombination, as described
657 (35). Suicide plasmid pJEH040 carries an approximately 1 kb SOE deletion fragment of
658 *pdhS2* on a pNPTS138 vector backbone. pNPTS138 is a ColE1 plasmid and as such is
659 unable to replicate in *A. tumefaciens*. pJEH040 was delivered to recipient strains by
660 either transformation or conjugation followed by selection on ATGN plates
661 supplemented with 300 $\mu g \cdot mL^{-1}$ Km, selecting for *A. tumefaciens* cells in which
662 pJEH040 had integrated at the chromosomal *pdhS2* locus by homologous
663 recombination. Recombinants were then grown overnight at 28°C in ATGN in the
664 absence of Km and plated the following day onto ATSN (ATGN with sucrose substituted
665 for glucose) agar plates to select for sucrose resistant (Suc^R) allelic replacement

bioRxiv preprint doi: https://doi.org/10.1101/148429; this version posted March 30, 2018. The copyright holder for this preprint (which was not certified by peer review) is the author/funder, who has granted bioRxiv a license to display the preprint in perpetuity. It is made available under aCC-BY-NC-ND 4.0 International license.

candidates. After three days' growth at 28°C colonies were patched in parallel onto ATGN Km and ATSN plates. Km^S Suc^R recombinants were then tested for the targeted deletion by diagnostic PCR using primers external to the *pdhS2* locus (JEH100 and JEH113) as well as internal primers (JEH85 and JEH87). Candidate colonies were further streak purified and verified a second time by diagnostic PCR before being used in downstream assays. Non-polar, markerless deletion of *dgcB* (Atu1691) in the Δ*pleD* and and Δ*pdhS2*Δ*pleD* genetic backgrounds was achieved using the above strategy with the pNPTS138 derivative pJX802.

Site-directed mutagenesis of *pdhS2* was achieved using mutagenic primer pairs JEH245/JEH246 (for generating the His271Ala allele, H271A) or JEH261/JEH262 (for generating the Thr275Ala allele, T275A). Plasmid pJEH021 carrying the wild-type *pdhS2* sequence was amplified by PCR using the above primer pairs. Following amplification, reaction mixtures were treated with *Dpn*I restriction endonuclease to remove template plasmid and then transformed into TOP10 F' *E. coli* competent cells. Purified plasmids from each transformation were sequenced and those containing the desired mutations, pJEH091 for His271Ala and pJEH099 for Thr275Ala, were selected for sub-cloning. pJEH091 and pJEH099 were digested with *Nde*I and *Nhe*I followed by gel electrophoresis and purification of the resulting insert. Inserts were ligated into similarly digested pSRKGm and transformed into competent *E. coli* TOP10 F' cells. Purified plasmids from each transformation were sequenced to verify their identity. The resulting plasmids, pJEH092 (H271A) and pJEH102 (T275A), were used to transform *A. tumefaciens*. To generate a PdhS2 allele carrying both H271A and T275A mutations the same steps were followed as above using plasmid pJEH091 as template with

bioRxiv preprint doi: https://doi.org/10.1101/148429; this version posted March 30, 2018. The copyright holder for this preprint (which was not certified by peer review) is the author/funder, who has granted bioRxiv a license to display the preprint in perpetuity. It is made available under aCC-BY-NC-ND 4.0 International license.

mutagenic primers JEH261/JEH262. Site-directed mutagenesis of the second CtrA half-site (5'-TTAA-3' → 5'-AATT-3') located 126 bp upstream of the start codon was performed as above using mutagenic primer pairs USP073/USP074 and plasmid pJX162 as template.

Translational fusions of full-length wild-type PdhS2 and DivJ to GFP were constructed as follows. *pdhS2* and *divJ*, each lacking a stop codon were amplified by PCR using primer pairs JEH65/JEH146 (*pdhS2*) and JEH147/JEH148 (*divJ*) with *A. tumefaciens* strain C58 genomic DNA as template. Primer design for these amplifications included 5' *Nde*I and 3' *Nhe*I restriction sites. The *gfpmut3* gene including a 5' *Nhe*I site and a 3' *Kpn*I site was amplified using primer pair JEH149/JEH150 and pJZ383 as template. Amplicons were gel purified, ligated into pGEM-T Easy, transformed into competent TOP10 F' *E. coli*, and eventually sequenced. The resulting plasmids, pJEH052 (*pdhS2*), pJEH053 (*gfpmut3*), and pJEH054 (*divJ*) were digested with either *Nde*I and *Nhe*I (pJEH052 and pJEH054) or *Nhe*I and *Kpn*I (pJEH053). Inserts were gel purified and used in a three-component ligation with *Nde*I/*Kpn*I-digested pSRKGm generating pJEH060 (PdhS2-GFP) and pJEH078 (DivJ-GFP). Sequenced plasmids were used to transform *A. tumefaciens*.

Reporter gene fusion constructs included predicted promoter regions from between 200 bp and 400 bp upstream of the indicated gene through the start codon. Each upsream region was amplified by PCR using the primers listed in Table S3 using *A. tumefaciens* genomic DNA as template. Amplicons were gel purified, ligated into pGEM-T Easy, transformed into competent TOP10 F' *E. coli*, and eventually sequenced. The resulting plasmids, pJEH113 (*ccrM*, Atu0794, promoter), pJEH115

bioRxiv preprint doi: https://doi.org/10.1101/148429; this version posted March 30, 2018. The copyright holder for this preprint (which was not certified by peer review) is the author/funder, who has granted bioRxiv a license to display the preprint in perpetuity. It is made available under aCC-BY-NC-ND 4.0 International license.

712 (*ctrA*, Atu2434, promoter), and pJEH119 (*pdhS1*, Atu0614, promoter) were digested
713 with either *Kpn*I and *Hin*DIII (pJEH113 and pJEH119) or *Kpn*I and *Pst*I (pJEH115).
714 Inserts were gel purified and ligated with similarly cleaved pRA301 containing a
715 promoterless *E. coli lacZ* gene without its own ribosome binding site. The resulting
716 constructs (pJEH121, pJEH122, and pJEH124) carry *lacZ* translationally fused to the
717 start codon for each gene with transcription and translation driven by the fused
718 upstream region. pJEH121, pJEH122, and pJEH124 were used to transform *A.*
719 *tumefaciens* for subsequent beta-galactosidase assays.
720
721 **Static biofilm assays.** Overnight cultures in ATGN were sub-cultured in fresh ATGN to
722 an optical density at 600 nm (OD_{600}) of 0.1 and grown with aeration at 28°C until an
723 OD_{600} of 0.25-0.6. Cultures were diluted to OD_{600} of 0.05 and 3 mL were inoculated into
724 each of four wells in a 12-well plate. A single coverslip was placed vertically into each
725 well to submerge approximately half of each coverslip. Plates were incubated in a
726 humidified chamber at 28° for 48 h. Coverslips were removed from each well, rinsed
727 with water, and adherent biomass stained by 5 min immersion in a 0.1% (w/v) crystal
728 violet solution. Adsorbed crystal violet was solubilized by immersion in 1 mL 33% acetic
729 acid and the absorbance of this solution determined at 600 nm (A_{600}) on a Synergy HT
730 multi-detection microplate reader (Bio-Tek). Culture density for each sample was also
731 determined by measuring the OD_{600} of each culture. Data are typically presented as
732 A_{600}/OD_{600} ratios normalized to values obtained for the wild-type strain within each
733 experiment. ATGN was supplemented with antibiotics and 250 μM IPTG as appropriate.
734 Final inoculations also included supplemental $FeSO_4$ (22 μM). Each mutant was

bioRxiv preprint doi: https://doi.org/10.1101/148429; this version posted March 30, 2018. The copyright holder for this preprint (which was not certified by peer review) is the author/funder, who has granted bioRxiv a license to display the preprint in perpetuity. It is made available under aCC-BY-NC-ND 4.0 International license.

735 evaluated in three independent experiments each of which contained three technical
736 replicates.
737
738 **Motility assays.** Wet mounts of exponentially growing cultures were observed under
739 brightfield optics using a Zeiss Axioskop 40 equipped with an AxioCam MRm
740 monochrome digital camera. Swim plates containing 0.3% agarose in ATGN,
741 supplemented with 1 mM IPTG and antibiotics when appropriate, were inoculated with a
742 single colony of the indicated strain at a central point and incubated for 7 days at 28°C.
743 Swim ring diameters were measured daily for seven days. Each experimental condition
744 was tested in three independent experiments containing three technical replicates.
745
746 **Microscopy.** Cell morphology and localization of PdhS2-GFP and DivJ-GFP was
747 evaluated using a Nikon E800 fluorescence microscope equipped with a Photometrics
748 Cascade cooled CCD camera. Overnight cultures were grown in ATGN with gentamicin
749 and 250 μM IPTG. The following day each strain was sub-cultured to OD_{600} 0.1 and
750 then grown at 28°C with aeration until ~OD_{600} 0.5-0.8. The culture (0.5 μl) was
751 transferred to a 1% ATGN/agarose pad on a clean glass slide and a clean 22 x 22 mm
752 number 1.5 glass coverslip placed on top. Images were acquired using a 100X oil
753 immersion objective and phase contrast optics or epifluorescence with a FITC-HYQ
754 filter set (Nikon; excitation filter = 480/40 nm, dichromatic mirror = 505 nm, absorption
755 filter = 535/50 nm). Time-lapse microscopy utilized a Nikon Ti-E inverted fluorescence
756 microscope with a Plan Apo 60X/1.40 oil Ph3 DM objective, a DAPI/FITC/Cy3/Cy5 filter
757 cube, an Andor iXon3 885 EMCCD camera, and a Lumencor Spectra X solid state light

bioRxiv preprint doi: https://doi.org/10.1101/148429; this version posted March 30, 2018. The copyright holder for this preprint (which was not certified by peer review) is the author/funder, who has granted bioRxiv a license to display the preprint in perpetuity. It is made available under aCC-BY-NC-ND 4.0 International license.

758 engine at 20% power. For time-lapse imaging agarose pads included 250 μM IPTG and
759 coverslips were attached to the glass slide using a gas-permeable 1:1:1 mixture of
760 Vaseline, lanolin, and paraffin. Phase and fluorescence images were captured every 20
761 min for 8 h using a 60 ms (phase) or 2 s (fluorescence) exposure. Images were
762 analyzed using ImageJ (76-78).
763
764 **Transcriptional profiling.** Whole-genome transcriptional profiling using custom 60-
765 mer oligonucleotide microarrays was performed essentially as previously described
766 (79). Arrays were produced by Agilent Technologies, and consist of 8455 features that
767 represent 5338 predicted protein-encoding open reading frames, tRNA and rRNA
768 encoding genes, and 2,983 duplicate spots. Cultures of wild-type or the Δ*pdhS2* mutant
769 strain of *A. tumefaciens* strain C58 were grown overnight in ATGN to full turbidity and
770 then sub-cultured 1:150 into fresh ATGN for a second overnight growth. The following
771 morning a volume equivalent to 11 ml of OD_{600} 0.6 was prepared for RNA extraction
772 using RNAprotect Bacteria Reagent (QIAGEN, Germantown, MD) following the
773 manufacturer's protocol. RNA was extracted from these samples using QIAGEN RNA
774 midipreps (QIAGEN, Germantown, MD) following the manufacturer's protocol. DNA
775 contamination was removed by DNase digestion using the TURBO DNA-free kit
776 (Ambion, Austin, TX) with the incubation time extended to two hours. First strand cDNA
777 synthesis was performed using Invitrogen SuperScript Indirect Labeling Kit, and cDNA
778 was purified on Qiagen QIAQuick columns. cDNA was labeled with AlexaFluor 555 and
779 647 dyes using Invitrogen SuperScript cDNA Labeling Kit, and repurified on QIAQuick
780 columns. cDNA was quantified on a NanoDrop spectrophotometer. Hybridization

bioRxiv preprint doi: https://doi.org/10.1101/148429; this version posted March 30, 2018. The copyright holder for this preprint (which was not certified by peer review) is the author/funder, who has granted bioRxiv a license to display the preprint in perpetuity. It is made available under aCC-BY-NC-ND 4.0 International license.

781 reactions were performed using Agilent in situ Hybridization Kit Plus, boiled for 5 min at
782 95°C, applied to the printed arrays, and hybridized overnight at 65°C. Hybridized arrays
783 were washed with Agilent Wash Solutions 1 and 2, rinsed with acetonitrile, and
784 incubated in Agilent Stabilization and Drying Solution immediately prior to scanning the
785 arrays. Three independent biological replicates were performed, with one dye swap.
786 Hybridized arrays were scanned on a GenePix Scanner 4200 in the Center for
787 Genomics and Bioinformatics (CGB) at Indiana University. GenePix software was used
788 to define the borders of hybridized spots, subtract background, measure dye intensity at
789 each spot, and calculate the ratio of dye intensities for each spot. Analysis of the
790 scanned images was conducted using the LIMMA package in R/Bioconductor.
791 Background correction of the data was performed using the minimum method (80, 81).
792 The data was normalized within arrays with the LOESS method, and between arrays
793 with the quantile method. Statistical analysis was performed using linear model fitting
794 and empirical Bayesian analysis by least squares. Genes with significant *P* values (≤
795 0.05) and with $\log_2$ ratios of ≥ 0.50 or ≤ -0.50 (representing a fold-change of ± 1.4) are
796 reported here. Expression data have been deposited in the Gene Expression Omnibus
797 (GEO) database at the National Center for Biotechnology Information (NCBI) under
798 accession number GSE71267 (82).

799 β-galactosidase activity was measured using a modified protocol of Miller (83).
800 Cultures carrying transcriptional reporter plasmids were grown overnight in ATGN and
801 sub-cultured the following morning to OD_{600} 0.15. Diluted cultures were grown at 28°C
802 with aeration until reaching mid-exponential growth. Between 100 and 300 μL of
803 exponential phase culture was mixed with Z buffer (60 mM Na_2HPO_4, 40 mM NaH_2PO_4,

bioRxiv preprint doi: https://doi.org/10.1101/148429; this version posted March 30, 2018. The copyright holder for this preprint (which was not certified by peer review) is the author/funder, who has granted bioRxiv a license to display the preprint in perpetuity. It is made available under aCC-BY-NC-ND 4.0 International license.

804 10 mM KCl, 1 mM $MgSO_4$, pH 7.0) to a final volume of 1 mL (volume of culture = f) plus
805 two drops 0.05% sodium dodecyl sulfate and 3 drops $CHCl_3$. The amount of culture
806 volume used was calibrated to generate reaction times between 15 minutes and two
807 hours for cultures with activity. 0.1 mL of a 4 $mg \cdot mL^{-1}$ solution in Z buffer of the
808 colorimetric substrate 2-nitrophenyl β-D-galactopyranoside (ONPG) was added and the
809 time (t) required for the solution to turn yellow was recorded. The reaction was stopped
810 by addition of 1 M Na_2CO_3 and the absorbance at 420 nm (A_{420}) of each solution was
811 measured. Promoter activity is expressed in Miller units (MUs = [1000 x A_{420nm}]/[OD_{600nm}
812 x t x f]). Each mutant was tested in three independent experiments containing five
813 technical replicates.
814
815 **Protein stability assays.** Steady-state levels of CtrA were determined from stationary
816 phase cultures of wild-type, Δ*divK*, and Δ*pdhS2* strains of *A. tumefaciens*. Overnight
817 cultures of each strain were grown in TY broth at 28ºC with aeration to an OD_{600} > 1.
818 Two 1 mL aliquots were removed from each culture, pelleted by centrifugation (13,200 x
819 *g*, 2 min) and supernatants discarded. One of the resulting pellets was resuspended on
820 ice in 50 μL 100 mM Tris·HCl, pH 6.8, followed by 50 μL 2X SDS-PAGE loading buffer
821 (65.8 mM Tris·HCl, pH 6.8, 26.3% (v/v) glycerol, 2.1% (w/v) sodium dodecyl sulfate
822 (SDS), 0.01% (w/v) bromophenol blue), then stored frozen at -20ºC. The second pellet
823 was resuspended in 100 μL 1X protein assay buffer (32.9 mM Tris·HCl, pH 6.8,
824 1%SDS), boiled 10 minutes, and used for protein concentration determination using the
825 Pierce BCA Protein Assay Kit (Thermo Fisher Scientific), per manufacturer's
826 instructions. Frozen resuspended pellets were thawed on ice and β-mercaptoethanol

bioRxiv preprint doi: https://doi.org/10.1101/148429; this version posted March 30, 2018. The copyright holder for this preprint (which was not certified by peer review) is the author/funder, who has granted bioRxiv a license to display the preprint in perpetuity. It is made available under aCC-BY-NC-ND 4.0 International license.

added to a final concentration of 5% prior to electrophoresis. Samples were normalized for protein concentration and separated on a 12.5% SDS-polyacrylamide gel. Following electrophoresis proteins were transferred to Immobilon-FL polyvinyl difluoride membranes (EMD Millipore). Membranes were rinsed in 1X Tris-buffered saline (TBS; 50 mM Tris·HCl, pH 7.5, 150 mM NaCl) solution and air dried. Membranes were wetted with MeOH and incubated in blocking buffer (1X TBS, 5% non-fat dairy milk [NFDM]) for 1 h at room temperature and then incubated overnight at 4ºC with primary antibody (1:5000 dilution of rabbit anti-CtrA from *C. crescentus,* anti-$CtrA_{Cc}$, in 1X TBS/5% NFDM/0.2% Tween 20). The following day membranes were rinsed thoroughly with 1X TBS/0.1% Tween 20 and incubated 1 h at room temperature with secondary antibody (1:20,000 dilution of IRDye 800CW-conjugated goat anti-rabbit antibody (LI-COR) in 1X TBS/5% NFDM/0.2% Tween 20/0.01% SDS). Membranes were rinsed thoroughly with 1X TBS/0.1% Tween 20 followed by 1X TBS alone and air dried in the dark. The resulting blot was imaged using a LI-COR Odyssey Classic infrared imaging system. Band intensities were quantified using the Odyssey Classic software.

Proteolytic turnover of CtrA was evaluated using translational shut-off assays. Overnight cultures were grown in TY broth at 28ºC with aeration. The following day each strain was sub-cultured in fresh TY broth to an OD_{600} 0.05 and incubated at 28ºC with aeration. To inhibit protein synthesis 90 $\mu g \cdot mL^{-1}$ chloramphenicol was added to each culture at OD_{600} 0.5. Starting at the time of chloramphenicol addition 5 mL aliquots were removed every 30 min for 3 h. Each aliquot was pelleted by centrifugation (5000 x *g*, 10 min). Cleared supernatants were discarded and pellets resuspended to an OD_{600} 10.0 in Tris-Cl, (10 mM, pH 8.0). Resuspended pellets were mixed with 2X SDS-PAGE

bioRxiv preprint doi: https://doi.org/10.1101/148429; this version posted March 30, 2018. The copyright holder for this preprint (which was not certified by peer review) is the author/funder, who has granted bioRxiv a license to display the preprint in perpetuity. It is made available under aCC-BY-NC-ND 4.0 International license.

loading buffer and stored frozen at -20ºC. Levels of CtrA were determined by SDS-PAGE and Western blotting as described above. Band intensities were quantified using the Odyssey Classic software and normalized to the band intensity of CtrA from the wild-type background at t = 0 min.

Global cdGMP measurement. Measurement of cdGMP levels was performed by liquid chromatography, tandem mass spectrometry (LC-MS/MS) on a Quattro Premier XE mass spectrometer coupled with an Acquity Ultra Performance LC system (Waters Corporation), essentially as previously described (84). Concentrations of cdGMP in cell samples were compared to chemically synthesized cdGMP (Axxora) dissolved in water at concentrations of 250, 125, 62.5, 31.2, 15.6, 7.8, 3.9, and 1.9 nM to generate a calibration curve. *A. tumefaciens* derivatives were grown in ATGN overnight at 28ºC to stationary phase. Culture densities were normalized after collecting cells by centrifugation and then resuspension in the appropriate volume of ATGN. Cultures were then pelleted by centrifugation and resuspended in ice-cold 250 μL extraction buffer (methanol:acetonitrile:water, 40:40:20 + 0.1 N formic acid) and incubated for 30 min at -20ºC. Resuspensions were transferred to microcentrifuge tubes and pelleted (13,000 x rpm, 5 min). 200 μL of the resulting supernatant was neutralized with 8 μL 15% NH_4HCO_3. Neutralized samples were stored at -20ºC. Prior to mass spectrometric analysis, samples were vacuum centrifuged to remove extraction buffer and resuspended in an equal volume of deionized water.

bioRxiv preprint doi: https://doi.org/10.1101/148429; this version posted March 30, 2018. The copyright holder for this preprint (which was not certified by peer review) is the author/funder, who has granted bioRxiv a license to display the preprint in perpetuity. It is made available under aCC-BY-NC-ND 4.0 International license.

872 ## ACKNOWLEDGEMENTS

873 This project was supported by National Institutes of Health (NIH) grants GM080546 and
874 GM120337 (C.F.) and GM109259 (C.M.W.). J.E.H. was supported by a Ruth L.
875 Kirschstein National Research Service Award (1 F32 GM100601) from the NIH and the
876 Milton Lev Memorial Faculty Research Fund from University of the Sciences in
877 Philadelphia. The authors thank Peter Chien (U. Mass. Amherst) for generously
878 providing the $CtrA_{Cc}$ antibody, and the Brun laboratory for access to and training on the
879 Nikon E800 microscope.

880

bioRxiv preprint doi: https://doi.org/10.1101/148429; this version posted March 30, 2018. The copyright holder for this preprint (which was not certified by peer review) is the author/funder, who has granted bioRxiv a license to display the preprint in perpetuity. It is made available under aCC-BY-NC-ND 4.0 International license.

REFERENCES

1. **Kysela DT, Randich AM, Caccamo PD, Brun YV**. 2016. Diversity takes shape: understanding the mechanistic and adaptive basis of bacterial morphology. PLoS Biol **14**:e1002565.
2. **Dworkin M**. 1985. Developmental biology of the bacteria. Benjamin/Cummings Pub. Co., Reading, Mass.
3. **Hajduk IV, Rodrigues CD, Harry EJ**. 2016. Connecting the dots of the bacterial cell cycle: Coordinating chromosome replication and segregation with cell division. Semin Cell Dev Biol **53**:2-9.
4. **Costerton JW, Lewandowski Z, Caldwell DE, Korber DR, Lappin-Scott HM**. 1995. Microbial biofilms. Annu Rev Microbiol **49**:711-45.
5. **Jonas K**. 2014. To divide or not to divide: control of the bacterial cell cycle by environmental cues. Curr Opin Microbiol **18**:54-60.
6. **Brown PJ, de Pedro MA, Kysela DT, Van der Henst C, Kim J, De Bolle X, Fuqua C, Brun YV**. 2012. Polar growth in the Alphaproteobacterial order Rhizobiales. Proc Natl Acad Sci U S A **109**:1697-701.
7. **Zupan JR, Cameron TA, Anderson-Furgeson J, Zambryski PC**. 2013. Dynamic FtsA and FtsZ localization and outer membrane alterations during polar growth and cell division in *Agrobacterium tumefaciens*. Proc Natl Acad Sci U S A **110**:9060-5.
8. **Reuter SH, Shapiro L**. 1987. Asymmetric segregation of heat-shock proteins upon cell division in *Caulobacter crescentus*. J Mol Biol **194**:653-62.
9. **Lindner AB, Madden R, Demarez A, Stewart EJ, Taddei F**. 2008. Asymmetric segregation of protein aggregates is associated with cellular aging and rejuvenation. Proc Natl Acad Sci U S A **105**:3076-81.
10. **Kysela DT, Brown PJ, Huang KC, Brun YV**. 2013. Biological consequences and advantages of asymmetric bacterial growth. Annu Rev Microbiol **67**:417-35.
11. **Berne C, Ma X, Licata NA, Neves BR, Setayeshgar S, Brun YV, Dragnea B**. 2013. Physiochemical properties of *Caulobacter crescentus* holdfast: a localized bacterial adhesive. J Phys Chem B **117**:10492-503.
12. **Curtis PD, Brun YV**. 2010. Getting in the loop: regulation of development in *Caulobacter crescentus*. Microbiol Mol Biol Rev **74**:13-41.
13. **Quon KC, Marczynski GT, Shapiro L**. 1996. Cell cycle control by an essential bacterial two-component signal transduction protein. Cell **84**:83-93.
14. **Domian IJ, Reisenauer A, Shapiro L**. 1999. Feedback control of a master bacterial cell-cycle regulator. Proc Natl Acad Sci U S A **96**:6648-53.
15. **Lasker K, Mann TH, Shapiro L**. 2016. An intracellular compass spatially coordinates cell cycle modules in Caulobacter crescentus. Curr Opin Microbiol **33**:131-139.
16. **Jenal U, Fuchs T**. 1998. An essential protease involved in bacterial cell-cycle control. EMBO J **17**:5658-69.
17. **Siam R, Marczynski GT**. 2000. Cell cycle regulator phosphorylation stimulates two distinct modes of binding at a chromosome replication origin. EMBO J **19**:1138-47.
18. **Wheeler RT, Shapiro L**. 1999. Differential localization of two histidine kinases controlling bacterial cell differentiation. Mol Cell **4**:683-94.
19. **Viollier PH, Sternheim N, Shapiro L**. 2002. Identification of a localization factor for the polar positioning of bacterial structural and regulatory proteins. Proc Natl Acad Sci U S A **99**:13831-6.

bioRxiv preprint doi: https://doi.org/10.1101/148429; this version posted March 30, 2018. The copyright holder for this preprint (which was not certified by peer review) is the author/funder, who has granted bioRxiv a license to display the preprint in perpetuity. It is made available under aCC-BY-NC-ND 4.0 International license.

20. **Hinz AJ, Larson DE, Smith CS, Brun YV**. 2003. The *Caulobacter crescentus* polar organelle development protein PodJ is differentially localized and is required for polar targeting of the PleC development regulator. Mol Microbiol **47**:929-41.
21. **Radhakrishnan SK, Thanbichler M, Viollier PH**. 2008. The dynamic interplay between a cell fate determinant and a lysozyme homolog drives the asymmetric division cycle of *Caulobacter crescentus*. Genes Dev **22**:212-25.
22. **Paul R, Jaeger T, Abel S, Wiederkehr I, Folcher M, Biondi EG, Laub MT, Jenal U**. 2008. Allosteric regulation of histidine kinases by their cognate response regulator determines cell fate. Cell **133**:452-61.
23. **Tropini C, Huang KC**. 2012. Interplay between the localization and kinetics of phosphorylation in flagellar pole development of the bacterium *Caulobacter crescentus*. PLoS Comput Biol **8**:e1002602.
24. **Subramanian K, Paul MR, Tyson JJ**. 2013. Potential role of a bistable histidine kinase switch in the asymmetric division cycle of *Caulobacter crescentus*. PLoS Comput Biol **9**:e1003221.
25. **Subramanian K, Paul MR, Tyson JJ**. 2015. Dynamical localization of DivL and PleC in the asymmetric division cycle of *Caulobacter crescentus*: a theoretical investigation of alternative models. PLoS Comput Biol **11**:e1004348.
26. **Quon KC, Yang B, Domian IJ, Shapiro L, Marczynski GT**. 1998. Negative control of bacterial DNA replication by a cell cycle regulatory protein that binds at the chromosome origin. Proc Natl Acad Sci U S A **95**:120-5.
27. **Laub MT, Chen SL, Shapiro L, McAdams HH**. 2002. Genes directly controlled by CtrA, a master regulator of the Caulobacter cell cycle. Proc Natl Acad Sci U S A **99**:4632-7.
28. **Laub MT, McAdams HH, Feldblyum T, Fraser CM, Shapiro L**. 2000. Global analysis of the genetic network controlling a bacterial cell cycle. Science **290**:2144-8.
29. **Chen YE, Tsokos CG, Biondi EG, Perchuk BS, Laub MT**. 2009. Dynamics of two phosphorelays controlling cell cycle progression in *Caulobacter crescentus*. J Bacteriol **191**:7417-29.
30. **Dubey BN, Lori C, Ozaki S, Fucile G, Plaza-Menacho I, Jenal U, Schirmer T**. 2016. Cyclic di-GMP mediates a histidine kinase/phosphatase switch by noncovalent domain cross-linking. Sci Adv **2**:e1600823.
31. **Lori C, Ozaki S, Steiner S, Bohm R, Abel S, Dubey BN, Schirmer T, Hiller S, Jenal U**. 2015. Cyclic di-GMP acts as a cell cycle oscillator to drive chromosome replication. Nature **523**:236-9.
32. **Tsokos CG, Perchuk BS, Laub MT**. 2011. A dynamic complex of signaling proteins uses polar localization to regulate cell-fate asymmetry in *Caulobacter crescentus*. Dev Cell **20**:329-41.
33. **Childers WS, Xu Q, Mann TH, Mathews, II, Blair JA, Deacon AM, Shapiro L**. 2014. Cell fate regulation governed by a repurposed bacterial histidine kinase. PLoS Biol **12**:e1001979.
34. **Chen YE, Tropini C, Jonas K, Tsokos CG, Huang KC, Laub MT**. 2011. Spatial gradient of protein phosphorylation underlies replicative asymmetry in a bacterium. Proc Natl Acad Sci U S A **108**:1052-7.
35. **Kim J, Heindl JE, Fuqua C**. 2013. Coordination of division and development influences complex multicellular behavior in *Agrobacterium tumefaciens*. PLoS One **8**:e56682.
36. **Curtis PD, Brun YV**. 2014. Identification of essential alphaproteobacterial genes reveals operational variability in conserved developmental and cell cycle systems. Mol Microbiol **93**:713-35.
37. **Romling U, Galperin MY, Gomelsky M**. 2013. Cyclic di-GMP: the first 25 years of a universal bacterial second messenger. Microbiol Mol Biol Rev **77**:1-52.
38. **Gao R, Stock AM**. 2009. Biological insights from structures of two-component proteins. Annu Rev Microbiol **63**:133-54.

bioRxiv preprint doi: https://doi.org/10.1101/148429; this version posted March 30, 2018. The copyright holder for this preprint (which was not certified by peer review) is the author/funder, who has granted bioRxiv a license to display the preprint in perpetuity. It is made available under aCC-BY-NC-ND 4.0 International license.

39. **Huynh TN, Stewart V**. 2011. Negative control in two-component signal transduction by transmitter phosphatase activity. Mol Microbiol **82**:275-86.
40. **Gao R, Stock AM**. 2017. Quantitative kinetic analyses of shutting off a two-component system. MBio **8**.
41. **Hallez R, Bellefontaine AF, Letesson JJ, De Bolle X**. 2004. Morphological and functional asymmetry in alpha-proteobacteria. Trends Microbiol **12**:361-5.
42. **Pini F, Frage B, Ferri L, De Nisco NJ, Mohapatra SS, Taddei L, Fioravanti A, Dewitte F, Galardini M, Brilli M, Villeret V, Bazzicalupo M, Mengoni A, Walker GC, Becker A, Biondi EG**. 2013. The DivJ, CbrA and PleC system controls DivK phosphorylation and symbiosis in Sinorhizobium meliloti. Mol Microbiol **90**:54-71.
43. **Tsokos CG, Laub MT**. 2012. Polarity and cell fate asymmetry in *Caulobacter crescentus*. Curr Opin Microbiol **15**:744-50.
44. **Laloux G, Jacobs-Wagner C**. 2014. How do bacteria localize proteins to the cell pole? J Cell Sci **127**:11-9.
45. **Hallez R, Mignolet J, Van Mullem V, Wery M, Vandenhaute J, Letesson JJ, Jacobs-Wagner C, De Bolle X**. 2007. The asymmetric distribution of the essential histidine kinase PdhS indicates a differentiation event in *Brucella abortus*. EMBO J **26**:1444-55.
46. **Lam H, Matroule JY, Jacobs-Wagner C**. 2003. The asymmetric spatial distribution of bacterial signal transduction proteins coordinates cell cycle events. Dev Cell **5**:149-59.
47. **Ehrle HM, Guidry JT, Iacovetto R, Salisbury AK, Sandidge DJ, Bowman GR**. 2017. Polar organizing protein PopZ Is required for chromosome segregation in *Agrobacterium tumefaciens*. J Bacteriol **199**.
48. **Kahng LS, Shapiro L**. 2001. The CcrM DNA methyltransferase of *Agrobacterium tumefaciens* is essential, and its activity is cell cycle regulated. J Bacteriol **183**:3065-75.
49. **Brilli M, Fondi M, Fani R, Mengoni A, Ferri L, Bazzicalupo M, Biondi EG**. 2010. The diversity and evolution of cell cycle regulation in alpha-proteobacteria: a comparative genomic analysis. BMC Syst Biol **4**:52.
50. **Skerker JM, Shapiro L**. 2000. Identification and cell cycle control of a novel pilus system in *Caulobacter crescentus*. EMBO J **19**:3223-34.
51. **Stephens CM, Zweiger G, Shapiro L**. 1995. Coordinate cell cycle control of a *Caulobacter* DNA methyltransferase and the flagellar genetic hierarchy. J Bacteriol **177**:1662-9.
52. **Xu J, Kim J, Koestler BJ, Choi JH, Waters CM, Fuqua C**. 2013. Genetic analysis of *Agrobacterium tumefaciens* unipolar polysaccharide production reveals complex integrated control of the motile-to-sessile switch. Mol Microbiol **89**:929-48.
53. **Zhou B, Schrader JM, Kalogeraki VS, Abeliuk E, Dinh CB, Pham JQ, Cui ZZ, Dill DL, McAdams HH, Shapiro L**. 2015. The global regulatory architecture of transcription during the *Caulobacter* cell cycle. PLoS Genet **11**:e1004831.
54. **Heindl JE, Wang Y, Heckel BC, Mohari B, Feirer N, Fuqua C**. 2014. Mechanisms and regulation of surface interactions and biofilm formation in *Agrobacterium*. Front Plant Sci **5**:176.
55. **Douglas CJ, Staneloni RJ, Rubin RA, Nester EW**. 1985. Identification and genetic analysis of an *Agrobacterium tumefaciens* chromosomal virulence region. J Bacteriol **161**:850-60.
56. **Panis G, Murray SR, Viollier PH**. 2015. Versatility of global transcriptional regulators in alpha-Proteobacteria: from essential cell cycle control to ancillary functions. FEMS Microbiol Rev **39**:120-33.
57. **De Bolle X, Crosson S, Matroule JY, Letesson JJ**. 2015. *Brucella abortus* cell cycle and infection are coordinated. Trends Microbiol **23**:812-21.

bioRxiv preprint doi: https://doi.org/10.1101/148429; this version posted March 30, 2018. The copyright holder for this preprint (which was not certified by peer review) is the author/funder, who has granted bioRxiv a license to display the preprint in perpetuity. It is made available under aCC-BY-NC-ND 4.0 International license.

58. **Matroule JY, Lam H, Burnette DT, Jacobs-Wagner C**. 2004. Cytokinesis monitoring during development; rapid pole-to-pole shuttling of a signaling protein by localized kinase and phosphatase in *Caulobacter*. Cell **118**:579-90.
59. **Viollier PH, Sternheim N, Shapiro L**. 2002. A dynamically localized histidine kinase controls the asymmetric distribution of polar pili proteins. EMBO J **21**:4420-8.
60. **Radhakrishnan SK, Pritchard S, Viollier PH**. 2010. Coupling prokaryotic cell fate and division control with a bifunctional and oscillating oxidoreductase homolog. Dev Cell **18**:90-101.
61. **Pierce DL, O'Donnol DS, Allen RC, Javens JW, Quardokus EM, Brun YV**. 2006. Mutations in DivL and CckA rescue a *divJ* null mutant of *Caulobacter crescentus* by reducing the activity of CtrA. J Bacteriol **188**:2473-82.
62. **Schallies KB, Sadowski C, Meng J, Chien P, Gibson KE**. 2015. *Sinorhizobium meliloti* CtrA stability Is regulated in a CbrA-dependent manner that Is influenced by CpdR1. J Bacteriol **197**:2139-49.
63. **Jenal U, Reinders A, Lori C**. 2017. Cyclic di-GMP: second messenger extraordinaire. Nat Rev Microbiol **15**:271-284.
64. **Aldridge P, Paul R, Goymer P, Rainey P, Jenal U**. 2003. Role of the GGDEF regulator PleD in polar development of *Caulobacter crescentus*. Mol Microbiol **47**:1695-708.
65. **Lai TH, Kumagai Y, Hyodo M, Hayakawa Y, Rikihisa Y**. 2009. The *Anaplasma phagocytophilum* PleC histidine kinase and PleD diguanylate cyclase two-component system and role of cyclic di-GMP in host cell infection. J Bacteriol **191**:693-700.
66. **Hug I, Deshpande S, Sprecher KS, Pfohl T, Jenal U**. 2017. Second messenger-mediated tactile response by a bacterial rotary motor. Science **358**:531-534.
67. **Greene SE, Brilli M, Biondi EG, Komeili A**. 2012. Analysis of the CtrA pathway in *Magnetospirillum* reveals an ancestral role in motility in alphaproteobacteria. J Bacteriol **194**:2973-86.
68. **Wang H, Ziesche L, Frank O, Michael V, Martin M, Petersen J, Schulz S, Wagner-Dobler I, Tomasch J**. 2014. The CtrA phosphorelay integrates differentiation and communication in the marine alphaproteobacterium *Dinoroseobacter shibae*. BMC Genomics **15**:130.
69. **Zan J, Heindl JE, Liu Y, Fuqua C, Hill RT**. 2013. The CckA-ChpT-CtrA phosphorelay system is regulated by quorum sensing and controls flagellar motility in the marine sponge symbiont *Ruegeria* sp. KLH11. PLoS One **8**:e66346.
70. **Quinones-Valles C, Sanchez-Osorio I, Martinez-Antonio A**. 2014. Dynamical modeling of the cell cycle and cell fate emergence in *Caulobacter crescentus*. PLoS One **9**:e111116.
71. **Joshi KK, Berge M, Radhakrishnan SK, Viollier PH, Chien P**. 2015. An adaptor hierarchy regulates proteolysis during a bacterial cell cycle. Cell **163**:419-31.
72. **Kobayashi H, De Nisco NJ, Chien P, Simmons LA, Walker GC**. 2009. *Sinorhizobium meliloti* CpdR1 is critical for co-ordinating cell cycle progression and the symbiotic chronic infection. Mol Microbiol **73**:586-600.
73. **Wu J, Ohta N, Newton A**. 1998. An essential, multicomponent signal transduction pathway required for cell cycle regulation in *Caulobacter*. Proc Natl Acad Sci U S A **95**:1443-8.
74. **Tempe J, Petit A, Holsters M, Montagu MV, Schell J**. 1977. Thermosensitive step associated with transfer of Ti plasmid during conjugation - possible relation to transformation in crown gall. Proc. Natl. Acad. of Sci., USA **74**:2848-2849.
75. **Morton ER, Fuqua C**. 2012. Laboratory maintenance of *Agrobacterium*. Curr Protoc Microbiol **Chapter 1**:Unit3D 1.
76. **Schneider CA, Rasband WS, Eliceiri KW**. 2012. NIH Image to ImageJ: 25 years of image analysis. Nat Methods **9**:671-5.

bioRxiv preprint doi: https://doi.org/10.1101/148429; this version posted March 30, 2018. The copyright holder for this preprint (which was not certified by peer review) is the author/funder, who has granted bioRxiv a license to display the preprint in perpetuity. It is made available under aCC-BY-NC-ND 4.0 International license.

77. **Schindelin J, Arganda-Carreras I, Frise E, Kaynig V, Longair M, Pietzsch T, Preibisch S, Rueden C, Saalfeld S, Schmid B, Tinevez JY, White DJ, Hartenstein V, Eliceiri K, Tomancak P, Cardona A**. 2012. Fiji: an open-source platform for biological-image analysis. Nat Methods **9**:676-82.
78. **Schindelin J, Rueden CT, Hiner MC, Eliceiri KW**. 2015. The ImageJ ecosystem: An open platform for biomedical image analysis. Mol Reprod Dev **82**:518-29.
79. **Heindl JE, Hibbing ME, Xu J, Natarajan R, Buechlein AM, Fuqua C**. 2015. Discrete responses to limitation for iron and manganese in *Agrobacterium tumefaciens*: influence on attachment and biofilm formation. J Bacteriol **198**:816-29.
80. **Ritchie ME, Phipson B, Wu D, Hu Y, Law CW, Shi W, Smyth GK**. 2015. limma powers differential expression analyses for RNA-sequencing and microarray studies. Nucleic Acids Res **43**:e47.
81. R Core Team. 2016. R: A language and environment for statistical computing., *on* R Foundation for Statistical Computing. https://www.R-project.org. Accessed
82. **Edgar R, Domrachev M, Lash AE**. 2002. Gene Expression Omnibus: NCBI gene expression and hybridization array data repository. Nucleic Acids Res **30**:207-10.
83. **Miller JH**. 1972. Experiments in Molecular Genetics. Cold Spring Harbor, New York.
84. **Wang Y, Kim SH, Natarajan R, Heindl JE, Bruger EL, Waters CM, Michael AJ, Fuqua C**. 2016. Spermidine inversely influences surface interactions and planktonic growth in *Agrobacterium tumefaciens*. J Bacteriol **198**:2682-91.

bioRxiv preprint doi: https://doi.org/10.1101/148429; this version posted March 30, 2018. The copyright holder for this preprint (which was not certified by peer review) is the author/funder, who has granted bioRxiv a license to display the preprint in perpetuity. It is made available under aCC-BY-NC-ND 4.0 International license.

Tables

Table 1. Promoter activity of selected known and predicted CtrA-dependent promoters.[a]

Strain	Promoter source organism	Promoter	Activity (%WT ± SE)
WT	*C. crescentus*	*ccrM*	100 ± 1
		ctrA	100 ± 2
		pilA	100 ± 1
	A. tumefaciens	*ccrM*	100 ± 1
		ctrA	101 ± 1
		pdhS1	100 ± 1
		dgcB	100 ± 12
		Atu3318	104 ± 25
Δ*pdhS2*	*C. crescentus*	*ccrM*	109 ± 12
		ctrA	82 ± 4 [b]
		pilA	85 ± 2 [b]
	A. tumefaciens	*ccrM*	106 ± 2 [b]
		ctrA	84 ± 3 [b]
		pdhS1	119 ± 3 [b]
		dgcB	201 ± 26 [b]
		*dgcB**	156 ± 1 [c]
		Atu3318	352 ± 13 [b]
Δ*divK*	*C. crescentus*	*ccrM*	140 ± 6 [b]
		ctrA	132 ± 4 [b]
		pilA	99 ± 3
	A. tumefaciens	*ccrM*	116 ± 3 [b]
		ctrA	117 ± 2 [b]
		pdhS1	90 ± 1 [b]
		dgcB	68 ± 1 [b]
		*dgcB**	56 ± 1 [c]
		Atu3318	62 ± 1 [b]

[a] Promoter activity was measured as β-galactosidase activity of cell lysates from strains carrying either transcriptional (for *C. crescentus* promoters) or translational (for *A. tumefaciens* promoters) fusions of the indicated promoter regions to the *E. coli lacZ*

bioRxiv preprint doi: https://doi.org/10.1101/148429; this version posted March 30, 2018. The copyright holder for this preprint (which was not certified by peer review) is the author/funder, who has granted bioRxiv a license to display the preprint in perpetuity. It is made available under aCC-BY-NC-ND 4.0 International license.

gene. Activity for each promoter was normalized to activity in lysates from wild-type cells carrying the identical promoter. N = 9.

[b] $P < 0.05$ compared to WT value using Student's *t* test.

[c] *dgcB** indicates the same promoter region as for *dgcB* with mutation of the second CtrA half-site at -126 from 5'-TTAA-3' to 5'-AATT-3'. $P < 0.001$ compared to value for wild-type *dgcB* promoter in same strain background using Student's *t* test.

bioRxiv preprint doi: https://doi.org/10.1101/148429; this version posted March 30, 2018. The copyright holder for this preprint (which was not certified by peer review) is the author/funder, who has granted bioRxiv a license to display the preprint in perpetuity. It is made available under aCC-BY-NC-ND 4.0 International license.

1101 **Table 2. Differentially-regulated genes in the absence of *pdhS2*.[a]**

Locus	Gene	Product[b]	log_2 FC	CtrA binding site (+/-)[c]	CtrA half-site (+/-)[c]	Present in other PdhS arrays?[d]
Atu0461	-	*phage tail protein/type VI secretion system component*	2.42	(+) Atu8182[e]	+	no
Atu0227	-	tRNA-Leu	2.15	-	+	no
Atu5167	*avhB6*	type IV secretion protein	2.01	-	+	no
Atu2490	*asd*	aspartate semialdehyde dehydrogenase	1.93	-	+	no
Atu3318	-	LuxR family transcriptional regulator	1.84	+	+	no
Atu1471	*rluC*	ribosomal large subunit pseudouridine synthase C	1.84	-	+	no
Atu3755	*purK*	phosphoribosylaminoimidazole carboxylase ATPase subunit	1.70	-	+	no
Atu3606	*ftsE*	cell division ATP-binding protein	1.63	+	+	no
Atu1791	-	ABC transporter, membrane spanning protein (sugar)	1.55	-	+	no
Atu3572	-	XRE family transcriptional regulator	1.52	+	+	yes
Atu2217	-	*hypothetical protein*	1.52	-	+	no
Atu5119	*phoB*	two component response regulator	1.48	-	-	no
Atu3031	-	*hypothetical protein*	1.46	-	-	no
Atu1886	-	*DNA glycosylase*	1.41	-	-	no
Atu1964	-	tRNA-Trp	1.40	+	+	no
Atu1301	-	*Nudix hydrolase*	1.39	-	+	no
Atu3610	-	cation transporter	1.34	-	-	no
Atu6048	-	*RNA helicase*	1.32	-	+	no
Atu1691	*dgcB*	GGDEF family protein	1.32	+	+	no
Atu1887	*exoI*	succinoglycan biosynthesis protein	1.30	+	+	no
Atu1134	-	*lysyl-phosphatidylglycerol synthase*	1.30	-	-	no
Atu2665	-	MarR family transcriptional regulator	1.27	-	+	no
Atu2204	-	*hypothetical protein*	1.25	-	+	no
Atu0540	-	*hypothetical protein*	1.25	-	-	no
Atu4856	-	nucleotidyltransferase	-1.21	-	-	no
Atu4347	*tae*	type VI secreted effector	-1.23	(+) Atu4344	-	no
Atu4055	*exoK*	endo-1,3-1,4-beta-glycanase	-1.28	(+) Atu4056	+	yes
Atu4345	*tssD*	type VI secretion needle tube protein	-1.29	(+) Atu4344	+	no
Atu5091	*rcdB*	curdlan synthesis protein	-1.32	+	+	no
Atu4357	-	*transglutaminase-like Cys protease*	-1.34	-	+	yes

bioRxiv preprint doi: https://doi.org/10.1101/148429; this version posted March 30, 2018. The copyright holder for this preprint (which was not certified by peer review) is the author/funder, who has granted bioRxiv a license to display the preprint in perpetuity. It is made available under aCC-BY-NC-ND 4.0 International license.

Atu0343	*barA*	two component sensor kinase/response regulator hybrid	-1.37	-	-	no
Atu4053	*exoA*	succinoglycan biosynthesis protein	-1.42	(+) Atu4056	+	yes
Atu4056	*exoH*	succinoglycan biosynthesis protein	-1.42	+	+	yes
Atu3564	*exsH*	endo-1,3-1,4-beta-glycanase	-1.46	-	-	no
Atu3541	-	*transglutaminase-like Cys protease*	-1.51	-	+	no
Atu4627	-	*hypothetical protein*	-1.56	-	-	no
Atu4049	*exoP*	exopolysaccharide polymerization/transport protein	-1.64	(+) Atu4056	+	no
Atu1469	-	hypothetical protein	-1.80	+	+	no
Atu4050	*exoN*	UTP-glucose-1-phosphate uridylyltransferase	-1.82	(+) Atu4056	+	yes

[a] Gene expression was compared between WT and Δ*pdhS2* strains using whole-genome microarrays. Genes were defined as differentially regulated when the following conditions were met: $\log_2$ FC ≥ 0.50 OR $\log_2$ FC ≤ -0.50, AND $P < 0.050$, AND Q < 0.10.

[b] Predicted functions of hypothetical proteins, if available, are italicized.

[c] Intergenic regions 500 nt upstream and 100 nt downstream of start codon for each gene (or operon, if applicable) was scanned for possible CtrA binding sites, as described in the text.

[d] Results were compared with previously published *S. meliloti cbrA* and *divJ* microarrays and *C. crescentus divJ* and *pleC* microarrays, as described in the text.

[e] (+) with Atu number indicates that the putative CtrA box is located in the first gene of a predicted operon

bioRxiv preprint doi: https://doi.org/10.1101/148429; this version posted March 30, 2018. The copyright holder for this preprint (which was not certified by peer review) is the author/funder, who has granted bioRxiv a license to display the preprint in perpetuity. It is made available under aCC-BY-NC-ND 4.0 International license.

Figure Legends

Figure 1. The PdhS kinases of *C. crescentus* and *A. tumefaciens* differentially localize and affect phenotypic outputs through response regulators DivK, PleD, and CtrA. (A) Cartoon model of known localization of the namesake PdhS kinases from *C. crescentus*, PleC and DivJ, and three PdhS kinases from *A. tumefaciens*, PdhS1, PdhS2, and DivJ. Kinases represented as colored ovals with black border experimentally localize to the indicated poles. The PleC oval without a border has not been experimentally demonstrated to localize in *A. tumefaciens*. As a result of this localization phosphorylation status of direct PdhS kinase targets, DivK and PleD, and the indirect target, CtrA, may be differentially affected. (B) Multiple sequence alignment of the HisKA domain from the PdhS kinases of *C. crescentus* and *A. tumefaciens*. Sequences were aligned using the Clustal Omega web service hosted by the European Molecular Biology Laboratory (EMBL)-European Bioinformatics Institute. The four PdhS kinases from *A. tumefaciens* plus PleC and DivJ from *C. crescentus* were included. Also included are two additional predicted PdhS kinases, CC_0652 and CC_1062, from *C. crescentus*. The EnvZ sensor kinase is included for comparison. Yellow highlighting indicates residues that define the PdhS kinases. The conserved histidine and threonine residues mutated in this work are in bold.

Figure 2. Evaluation of roles for PdhS2 kinase and phosphatase activities and genetic interactions with *divK*. (A) The ability of plasmid-borne wild-type PdhS2 (p-*pdhS2*), the kinase-null allele (p-*pdhS2*, K^-P^+), or the phosphatase-null allele (p-*pdhS2,* K^+P^-) to complement the Δ*pdhS2* biofilm formation (black bars) and swimming motility

bioRxiv preprint doi: https://doi.org/10.1101/148429; this version posted March 30, 2018. The copyright holder for this preprint (which was not certified by peer review) is the author/funder, who has granted bioRxiv a license to display the preprint in perpetuity. It is made available under aCC-BY-NC-ND 4.0 International license.

(white bars) phenotypes was evaluated using P_{lac}-driven expression of each allele. Static biofilm formation was measured after 48 h (black bars) and swim ring diameter after 7 days (white bars). Adherent biomass on PVC coverslips was determined by adsorption of crystal violet. Crystal violet was then solubilized and $A_{600\ nm}$ values were normalized to culture density (OD_{600}). Data are the mean of three independent experiments each of which contained three technical replicates (N = 3). Swim ring diameters were measured after single-colony inoculation into low density swim agar and incubation at room temperature. Data are the mean of nine independent experiments (N = 9). (B) Biofilm formation (black bars) and swimming motility (white bars) were evaluated in the indicated strains. Experiments were performed and data analyzed as described for (A) above. (C) The effect of plasmid-borne wild-type PdhS2 (p-*pdhS2*), the kinase-null allele (p-*pdhS2* (K^-P^+)), or the phosphatase-null allele (p-*pdhS2* (K^+P^-)) on biofilm formation (black bars) and swimming motility (white bars) when expressed from the P_{lac} promoter in the Δ*divK* mutant background was evaluated as in (A) and (B) above. For presentation all data are normalized to WT and expressed as %WT ± standard error of the mean (S.E.). ([a]) = $P < 0.05$ compared to wild-type strain or wild-type strain carrying empty vector. ([b]) = $P < 0.05$ compared to Δ*pdhS2* strain carrying empty vector (A), or compared to the Δ*pdhS2* mutant strain (B), or compared to the Δ*divK* strain carrying empty vector (C). Statistical significance was determined using Student's *t* test.

Figure 3. PdhS2 and DivJ are polarly localized in *A. tumefaciens*. Time-lapse microscopy of a C-terminal green fluorescent protein fusions to PdhS2 (A) and DivJ (B).

bioRxiv preprint doi: https://doi.org/10.1101/148429; this version posted March 30, 2018. The copyright holder for this preprint (which was not certified by peer review) is the author/funder, who has granted bioRxiv a license to display the preprint in perpetuity. It is made available under aCC-BY-NC-ND 4.0 International license.

Overlaid phase and fluorescent images, acquired sequentially on Nikon E800 fluorescence microscope with a CCD camera using the 100 X objective. Time between panels is 40 minutes. To the right of each image is a cartoon interpretation of the image.

Figure 4. PdhS2 impacts CtrA abundance but not turnover kinetics. (A) Steady-state CtrA levels in indicated strains as determined via SDS-PAGE followed by immunoblotting with rabbit anti-$CtrA_{Cc}$ primary and IRDye 800CW-conjugated goat anti-rabbit secondary antibodies. (B) Proteolytic turnover of CtrA following translational arrest with chloramphenicol. Aliquots were removed at the indicated time points, lysed, and stored frozen at -20 ºC. CtrA levels were then determined via SDS-PAGE followed by immunoblotting, as described for (A) above. Blots were imaged using an LI-COR Odyssey Classic infrared imaging system and band intensities quantified with the Odyssey Classic software. Protein concentrations for each sample were normalized to optical density prior to electrophoresis.

Figure 5. PdhS2 intersects with the activity of multiple diguanylate cyclases. (A) Biofilm formation was quantified for the wild-type (WT) and indicated mutant strains as described in Figure 2. PleD, DgcA, DgcB have demonstrated *in vivo* diguanylate cyclase enzymatic activity. Thus far conditions under which DgcC is active have yet to be identified. $P < 0.05$ compared to WT ([a]), Δ*pdhS2* ([b]), or corresponding diguanylate cyclase ([c]). (B) The effect on biofilm formation of plasmid-borne expression of wild-type *dgcB* (p-*dgcB*) or a catalytic mutant allele of *dgcB* (p-*dgcB**) was evaluated. Expression

bioRxiv preprint doi: https://doi.org/10.1101/148429; this version posted March 30, 2018. The copyright holder for this preprint (which was not certified by peer review) is the author/funder, who has granted bioRxiv a license to display the preprint in perpetuity. It is made available under aCC-BY-NC-ND 4.0 International license.

of each *dgcB* allele was driven by the P_{lac} promoter. Biofilm formation was evaluated as described in Figure 2. (*) = $P < 0.05$ compared to vector alone.

Figure 6. An alternative model for PdhS2 regulation of CtrA activity. Our data are consistent with PdhS2 intersecting the DivK-CtrA regulatory pathway at one of two points. (Pathway A) Canonical genetic model with PdhS2 interacting with DivK. The phosphorylation status of DivK then modulates CtrA activity through the CckA-ChpT-CtrA axis. (Pathway B) DivK-independent model of CtrA regulation by PdhS2 through an unidentified response regulator, RR-X. Both routes to regulation of CtrA activity ultimately affect the phosphorylation status of CtrA, affecting occupancy at CtrA-regulated promoters, and finally leading to inverse regulation of attachment (primarily through cdGMP pools) and separately motility. Regulatory proteins: Blue text; histidine kinases; orange text, histidine phosphotransferase (Hpt); green text, response regulators. RR-X indicates a putative response regulator, yet to be identified.

bioRxiv preprint doi: https://doi.org/10.1101/148429; this version posted March 30, 2018. The copyright holder for this preprint (which was not certified by peer review) is the author/funder, who has granted bioRxiv a license to display the preprint in perpetuity. It is made available under aCC-BY-NC-ND 4.0 International license.

SUPPLEMENTARY MATERIAL

Reciprocal control of motility and biofilm formation by the PdhS2 two-component sensor kinase of *Agrobacterium tumefaciens*

Jason E. Heindl, Daniel Crosby, Sukhdev Brar, Tiyan Singletary, Daniel Merenich, Aaron M. Buechlein, Justin L. Eagan, Eric L. Bruger, Christopher M. Waters and Clay Fuqua

Running title: *Agrobacterium PdhS2 regulates motility and biofilms*

1) Supplementary Figures – S1-S10

2) Supplementary Figure Legends

3) Supplementary Tables – S1-S3

4) Supplementary References

bioRxiv preprint doi: https://doi.org/10.1101/148429; this version posted March 30, 2018. The copyright holder for this preprint (which was not certified by peer review) is the author/funder, who has granted bioRxiv a license to display the preprint in perpetuity. It is made available under aCC-BY-NC-ND 4.0 International license.

Figure S1. A combined kinase- and phosphatase-null PdhS2 mutant allele has little effect on biofilm formation or swimming motility. The ability of plasmid-borne expression of a kinase- and phosphatase- null allele of *pdhS2* (p-*pdhS2* (K^-P^-)) to complement the Δ*pdhS2* phenotypes was compared against the wild-type *pdhS2* allele (p-*pdhS2*). Biofilm formation (black bars) and swimming motility (white bars) were evaluated as in Figure 2. (^{a}) = $P < 0.05$ compared to the wild-type background with vector only; (^{b}) = $P < 0.05$ compared to the Δ*pdhS2* background with vector only. Statistical significance was determined using Student's *t* test.

Figure S2. Morphology of WT, Δ*divK*, Δ*pdhS2*, and Δ*divK* Δ*pdhS2* strains. Strains were grown to exponential phase in ATGN. Aliquots of cells were placed on top of an ATGN/1% agarose pad and imaged using phase contrast microscopy. (A), WT; (B) Δ*divK*; (C) Δ*pdhS2*; (D) Δ*divK* Δ*pdhS2*. Representative images are shown. Scale bar = 2 μm.

Figure S3. A kinase-locked allele of CckA fails to suppress the PdhS2-dependent biofilm phenotype. Biofilm formation was evaluated in the indicated strains as described in Figure 2. (*) = $P < 0.05$ compared to background strain carrying vector alone. Statistical significance was determined using Student's *t* test.

Figure S4. A kinase-locked allele of CckA fails to suppress the PdhS2-dependent swimming motility phenotype. Swimming motility was evaluated in the indicated

bioRxiv preprint doi: https://doi.org/10.1101/148429; this version posted March 30, 2018. The copyright holder for this preprint (which was not certified by peer review) is the author/funder, who has granted bioRxiv a license to display the preprint in perpetuity. It is made available under aCC-BY-NC-ND 4.0 International license.

strains as described in Figure 2. (*) = $P < 0.001$ compared to background strain carrying vector alone. Statistical significance was determined using Student's *t* test.

Figure S5. Predicted CtrA-dependent promoters bearing one or more CtrA binding motifs. Upstream regions from genes whose expression is increased (red) or decreased (black) in the Δ*pdhS2* mutant background relative to the wild-type background (microarray or *lacZ* fusion data). Predicted CtrA binding sites, as defined in the main text, are indicated. For genes in operons, the most upstream gene that has a predicted CtrA box is shown, even if this upstream gene did not make the expression cutoff for Table 2 (e.g. Atu4344 and Atu 8282). Only those genes with a predicted full CtrA binding site are shown.

Figure S6. PdhS2 regulation of swimming motility is independent of diguanylate cyclase activity. Swimming motility of the wild-type (WT) and indicated mutant strains was evaluated as described in Figure 2. $P < 0.05$ compared to WT ([a]), Δ*pdhS2* ([b]), or corresponding diguanylate cyclase ([c]).

Figure S7. Loss of *pdhS2* enhances biofilm formation in the absence of both *dgcB* and *pleD*. Biofilm formation and swimming motility was evaluated in the wild-type (WT) and indicated mutant strains as described in Figure 2. (*) = $P < 0.05$ compared to the wild-type background. Statistical significance was determined using Student's *t* test.

bioRxiv preprint doi: https://doi.org/10.1101/148429; this version posted March 30, 2018. The copyright holder for this preprint (which was not certified by peer review) is the author/funder, who has granted bioRxiv a license to display the preprint in perpetuity. It is made available under aCC-BY-NC-ND 4.0 International license.

Figure S8. PdhS2 does not affect global levels of cyclic-di-GMP. Cyclic-di-GMP levels were measured in whole cell extracts from equivalent ODs of the indicated strains. Data are from three independent experiments (N = 3).

Figure S9. A catalytically inactive DgcB does not affect swimming motility. The effect on swimming motility of plasmid-borne expression of wild-type *dgcB* (p-*dgcB*) or a catalytic mutant allele of *dgcB* (p-*dgcB**) was evaluated. Expression of each *dgcB* allele was driven by the P_{lac} promoter. Biofilm formation was evaluated as described in Figure 2. (*) = $P < 0.05$ compared to vector alone.

Figure S10. The unipolar polysaccharide is required for PdhS2-dependent biofilm formation. (A) Biofilm formation was evaluated in the presence (+) or absence (-) of *pdhS2* in combination with the indicated polysaccharides. WT = wild-type, Cel^- = cellulose mutant, $ChvAB^-$ = cyclic-β-glucan mutant, $CrdS^-$ = curdlan mutant, $ExoA^-$ = succinoglycan mutant, UPP^- = unipolar polysaccharide mutant, EPS^- = mutant lacking all of the above polysaccharides. (B) Swimming motility was evaluated in the same strains as in (A). (*) = $P < 0.05$ compared to background strain. Statistical significance was determined using Student's *t* test.

Figure S1

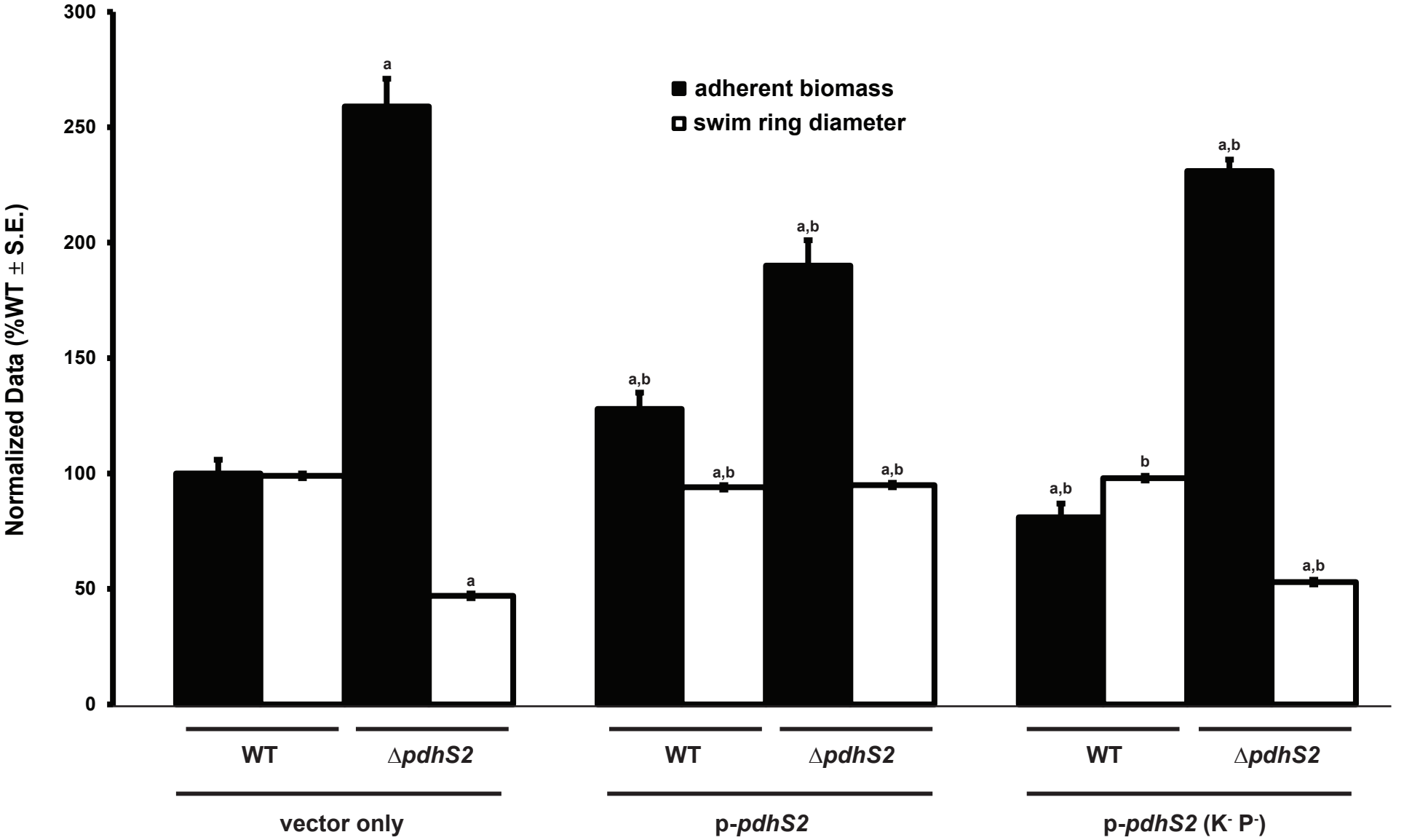
300
250
200
150
100
50
0
Normalized Data (%WT ± S.E.)
adherent biomass
swim ring diameter
a
a
a,b
a,b
a,b
a,b
a,b
b
a,b
WT
ΔpdhS2
WT
ΔpdhS2
WT
ΔpdhS2
vector only
p-pdhS2
p-pdhS2 (K- P-)

Figure S2

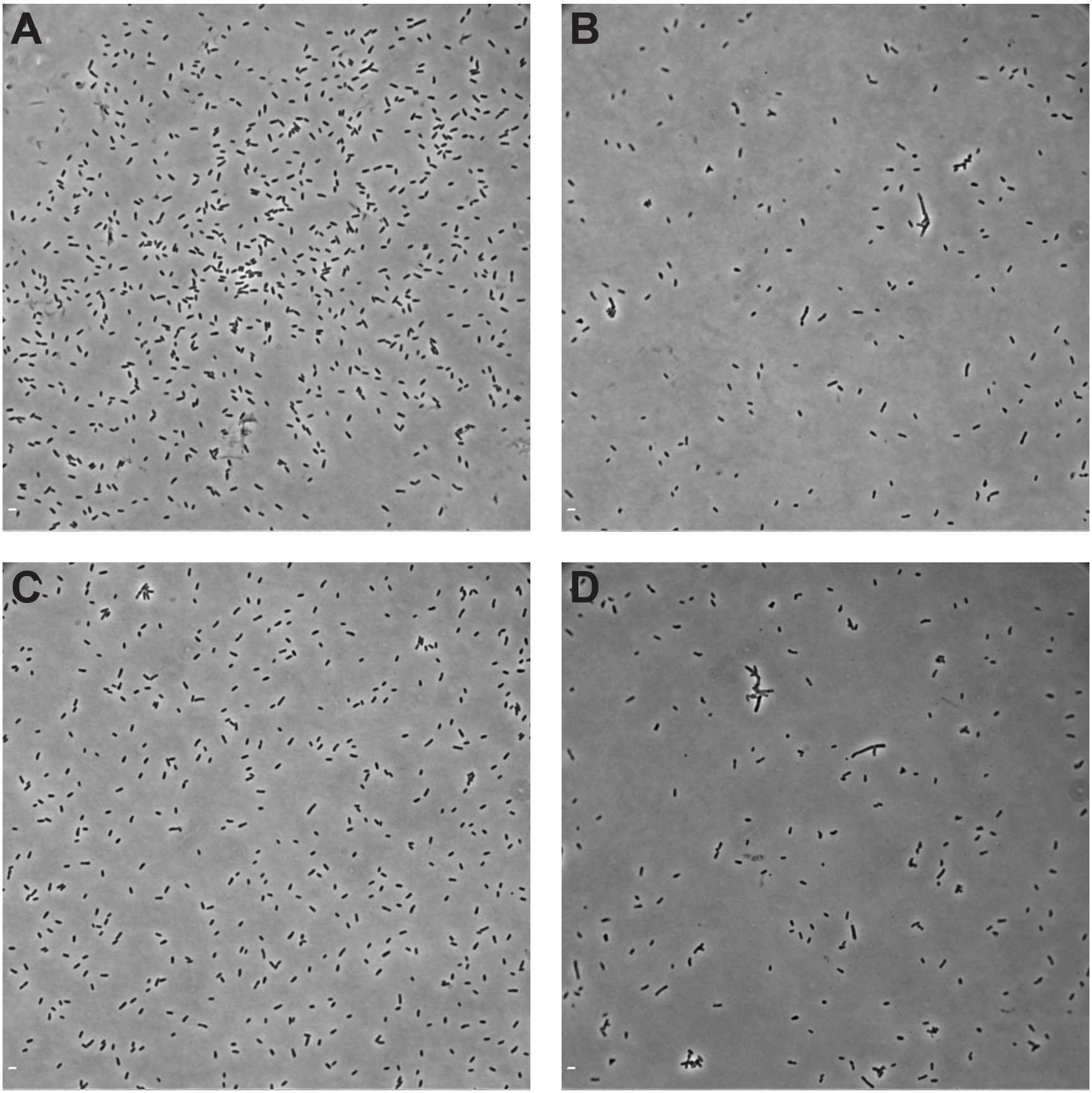

Figure S3

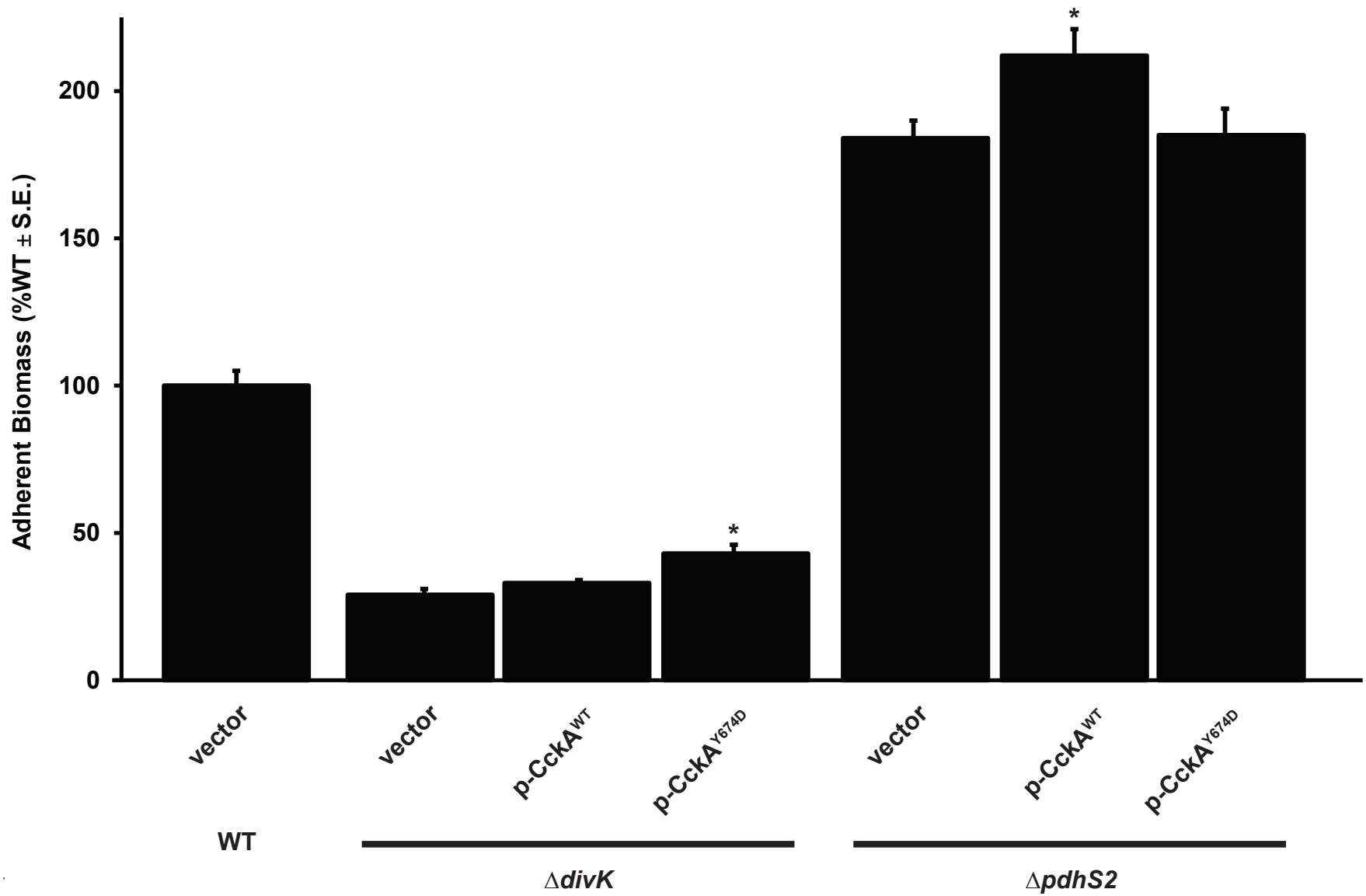
Adherent Biomass (%WT ± S.E.)
200
150
100
50
0
*
*
vector
vector
p-CckA^WT
p-CckA^Y674D
vector
p-CckA^WT
p-CckA^Y674D
WT
ΔdivK
ΔpdhS2

Figure S4

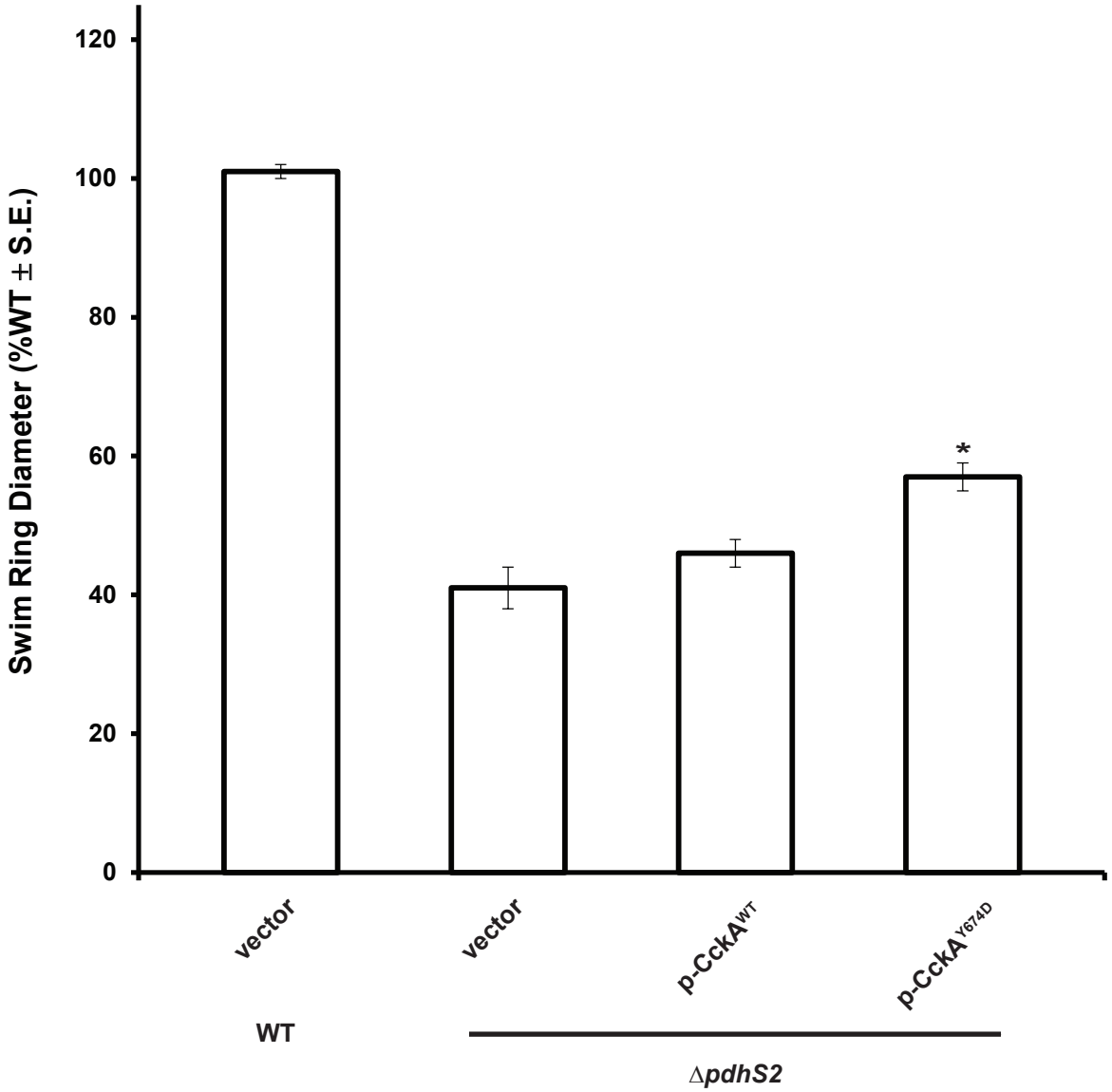
Swim Ring Diameter (%WT ± S.E.)
120
100
80
60
40
20
0
*
vector
vector
p-CckA^WT
p-CckA^Y674D
WT
ΔpdhS2

bioRxiv preprint doi: https://doi.org/10.1101/148429; this version posted March 30, 2018. The copyright holder for this preprint (which was not certified by peer review) is the author/funder, who has granted bioRxiv a license to display the preprint in perpetuity. It is made available under aCC-BY-NC-ND 4.0 International license.

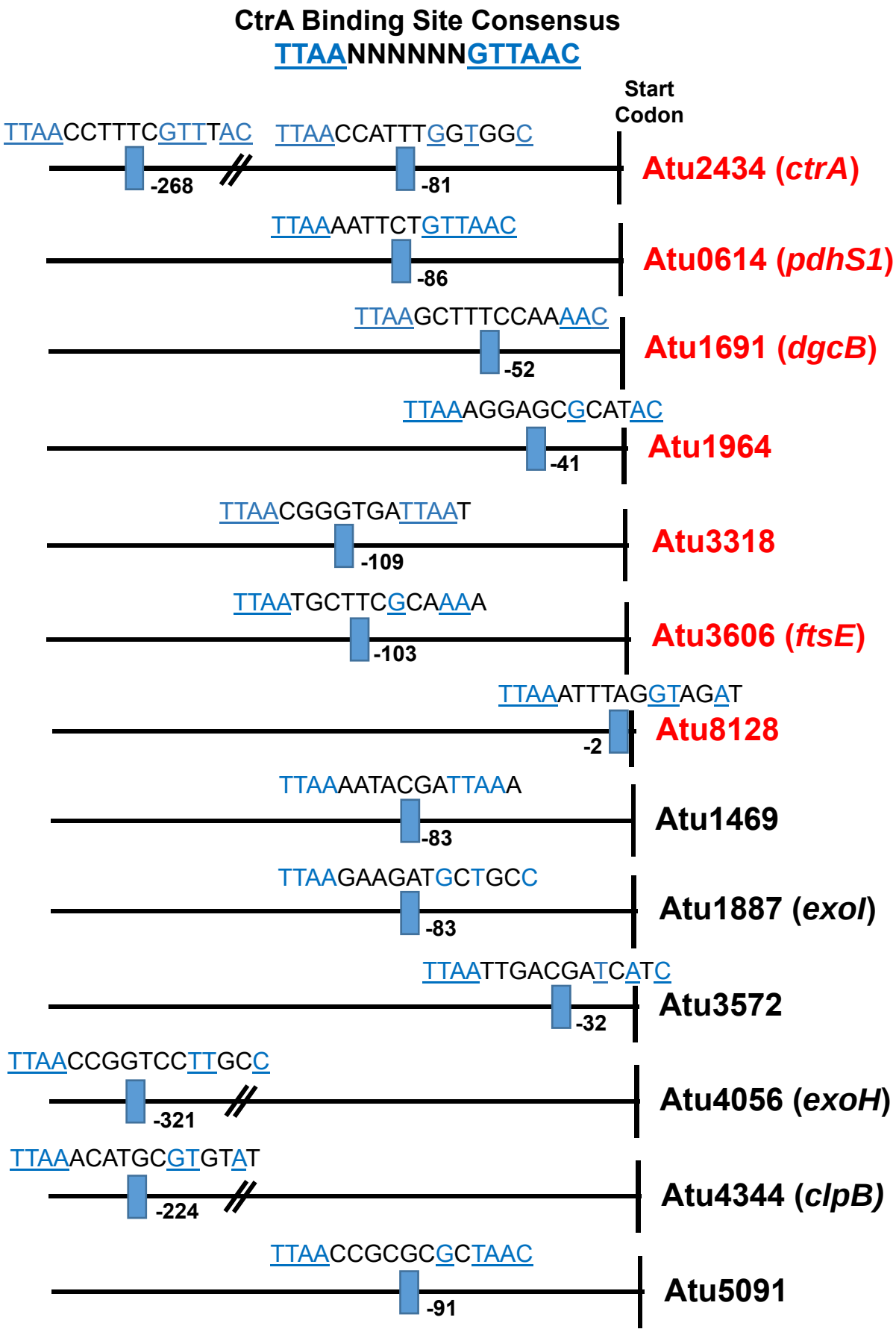

Figure S6

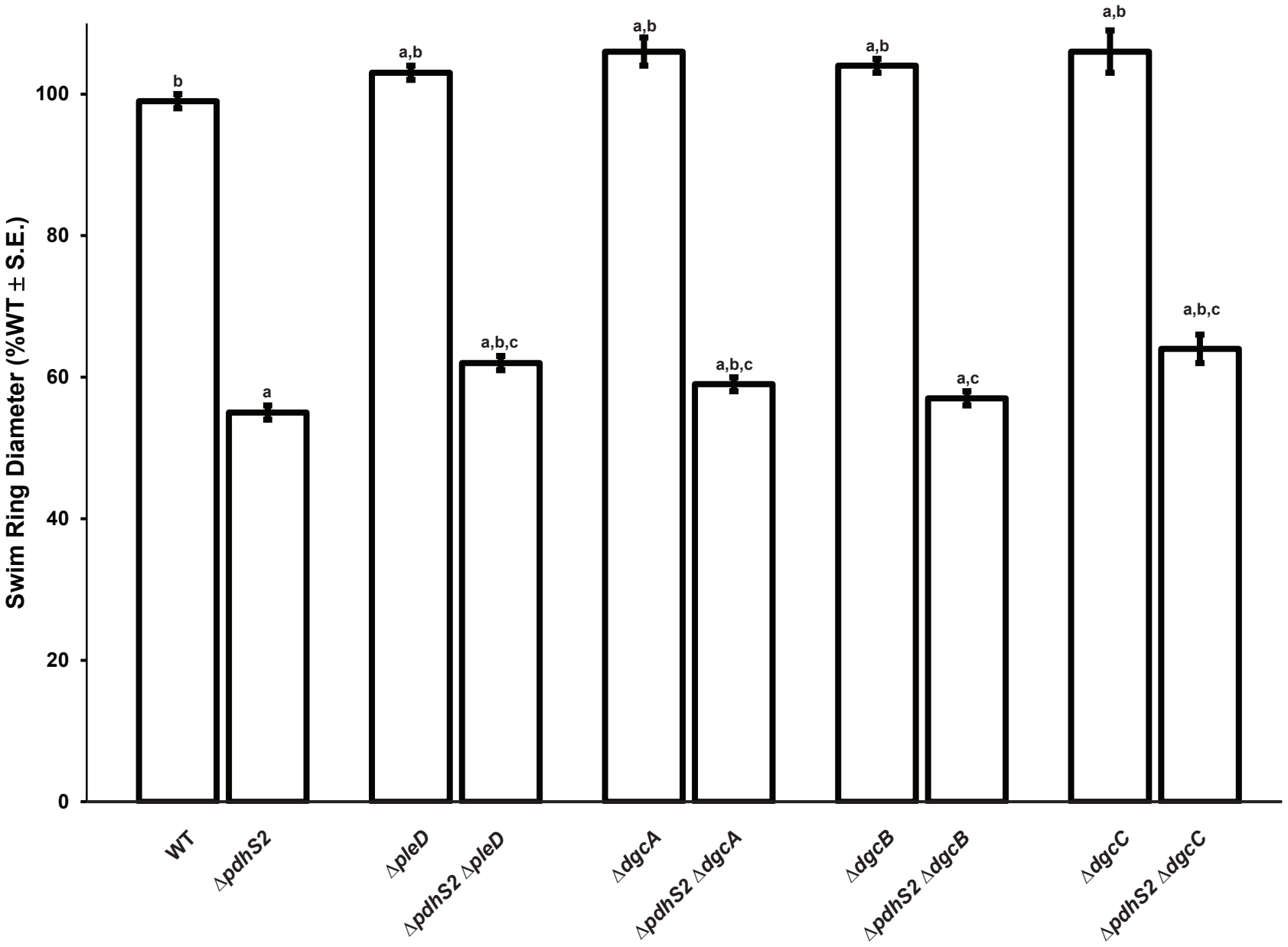
Swim Ring Diameter (%WT ± S.E.)
0
20
40
60
80
100
b
a
a,b
a,b,c
a,b
a,b,c
a,b
a,c
a,b
a,b,c
WT
ΔpdhS2
ΔpleD
ΔpdhS2 ΔpleD
ΔdgcA
ΔpdhS2 ΔdgcA
ΔdgcB
ΔpdhS2 ΔdgcB
ΔdgcC
ΔpdhS2 ΔdgcC

Figure S7

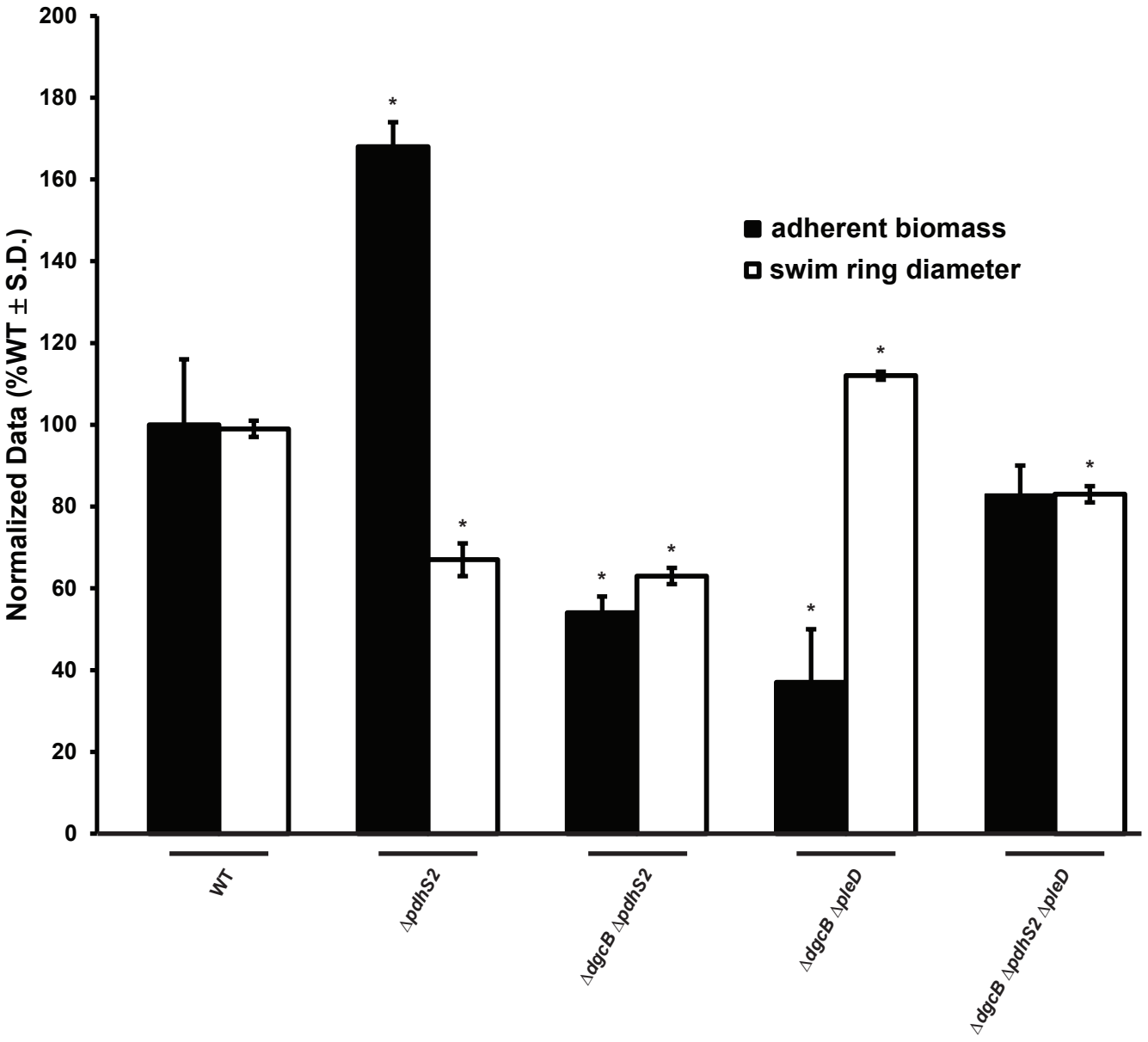
Normalized Data (%WT ± S.D.)
200
180
160
140
120
100
80
60
40
20
0
adherent biomass
swim ring diameter
*
WT
ΔpdhS2
ΔdgcB ΔpdhS2
ΔdgcB ΔpleD
ΔdgcB ΔpdhS2 ΔpleD

Figure S8

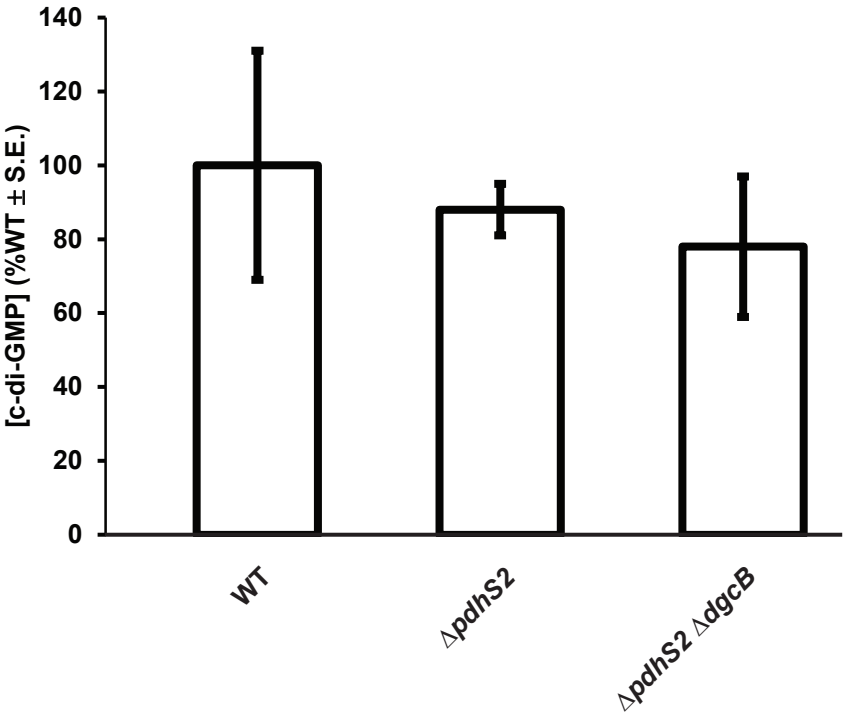

Figure S9

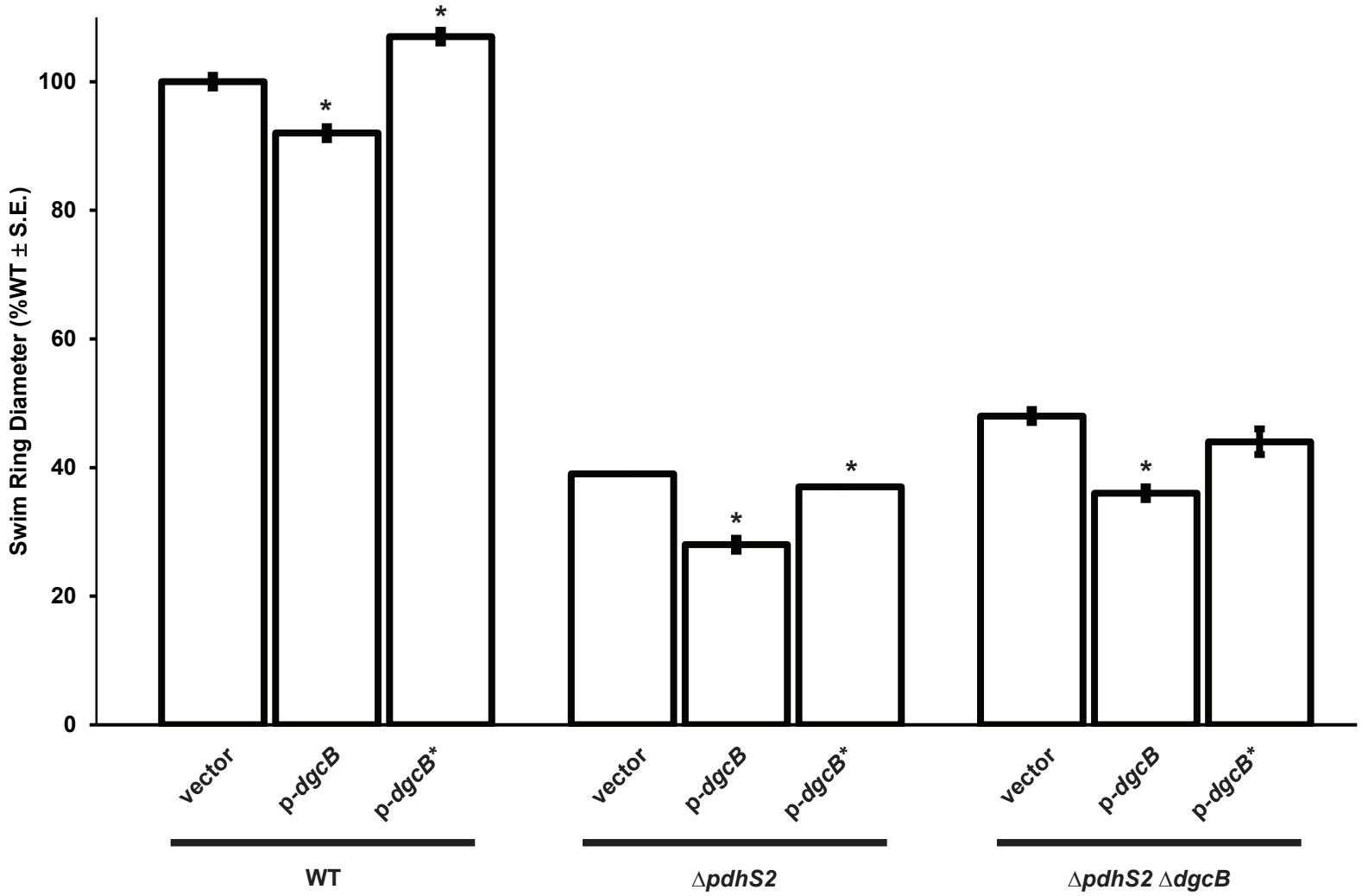
Swim Ring Diameter (%WT ± S.E.)
0
20
40
60
80
100
*
*
*
*
*
vector
p-dgcB
p-dgcB*
vector
p-dgcB
p-dgcB*
vector
p-dgcB
p-dgcB*
WT
ΔpdhS2
ΔpdhS2 ΔdgcB

Figure S10A

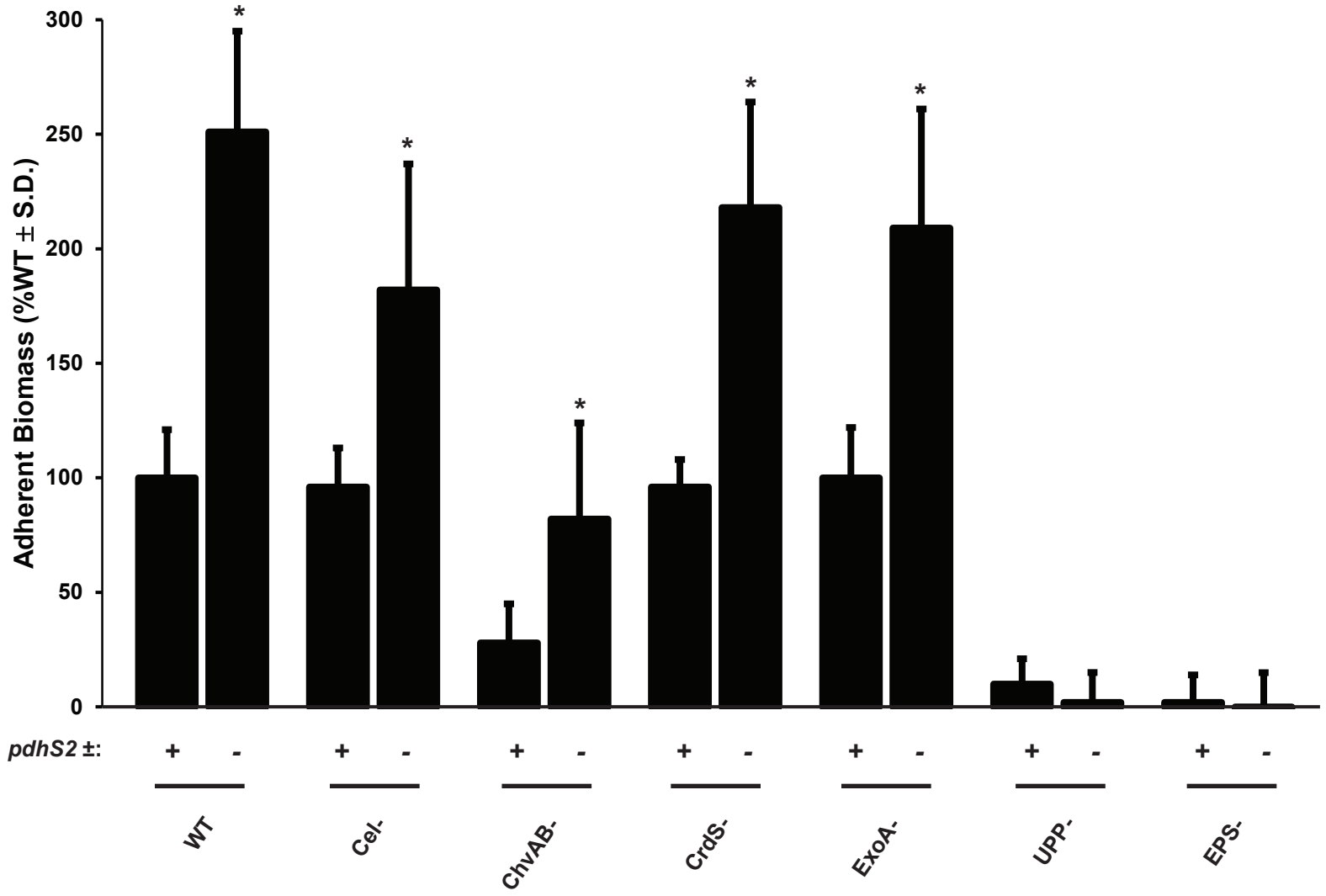
Adherent Biomass (%WT ± S.D.)
300
250
200
150
100
50
0
*
pdhS2 ±:
+
-
WT
Cel-
ChvAB-
CrdS-
ExoA-
UPP-
EPS-

Figure S10B

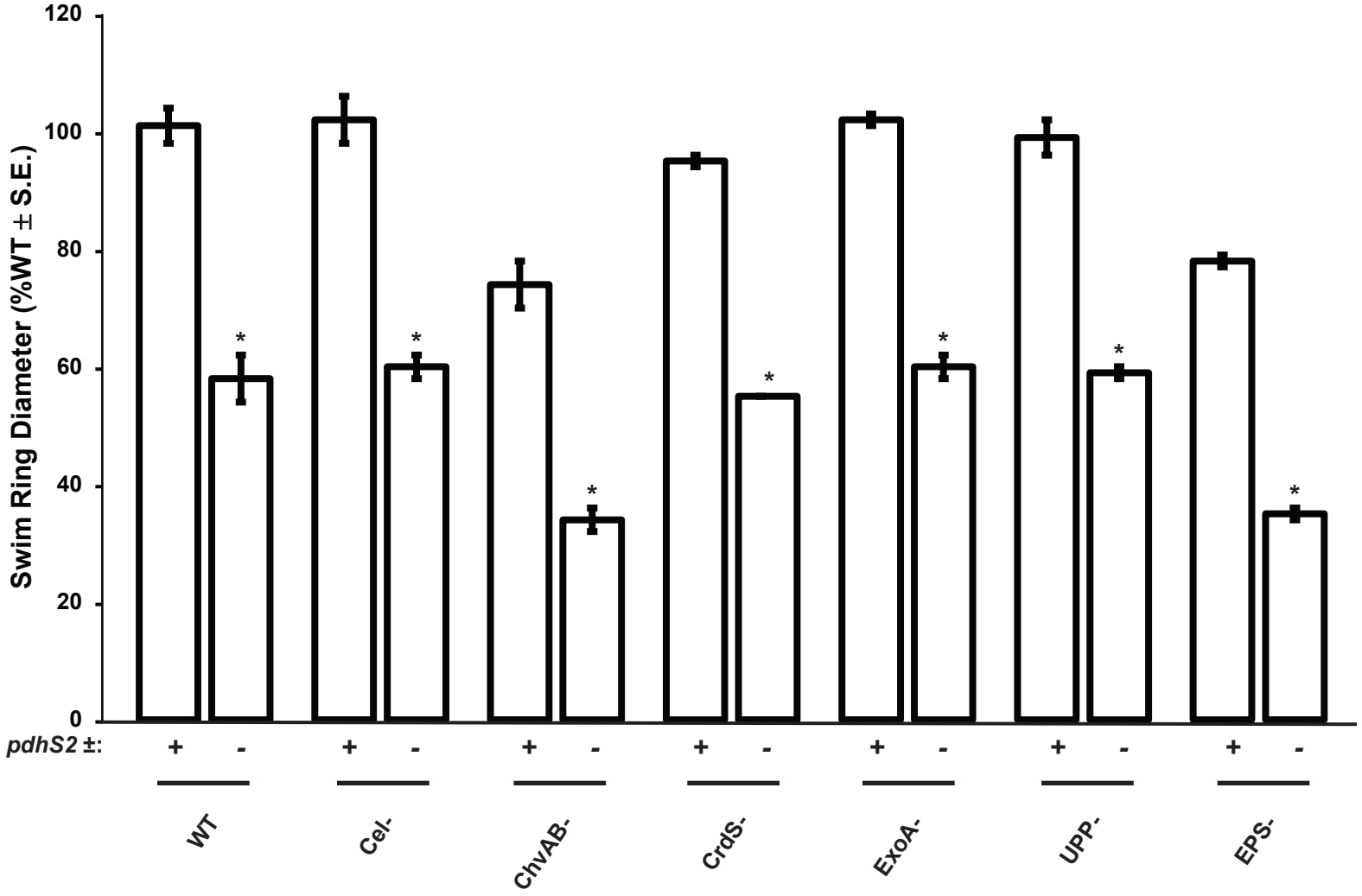
Swim Ring Diameter (%WT ± S.E.)
120
100
80
60
40
20
0
*
pdhS2 ±:
+
-
WT
Cel-
ChvAB-
CrdS-
ExoA-
UPP-
EPS-

bioRxiv preprint doi: https://doi.org/10.1101/148429; this version posted March 30, 2018. The copyright holder for this preprint (which was not certified by peer review) is the author/funder, who has granted bioRxiv a license to display the preprint in perpetuity. It is made available under aCC-BY-NC-ND 4.0 International license.

Table S1. Strains used in this study

Species	Strain	Relevant Characteristics	Source
A. tumefaciens	C58	Nopaline type strain, pAtC58, pTiC58	(1)
A. tumefaciens	C58-JE001	Δ*dgcB* Δ*pdhS2* Δ*pleD* (ΔAtu1691 ΔAtu1888 ΔAtu1297)	This study
A. tumefaciens	C58-JE002	Δ*dgcB* Δ*pleD* (ΔAtu1691 ΔAtu1297)	This study
A. tumefaciens	C58-JEH076	Δ*pdhS2* (ΔAtu1888)	(2)
A. tumefaciens	C58-JEH128	Δ*pdhS2* Δ*pleD* (ΔAtu1888 ΔAtu1297)	This study
A. tumefaciens	C58-JEH130	Δ*pdhS2* Δ*dgcA* (ΔAtu1888 ΔAtu1257)	This study
A. tumefaciens	C58-JEH131	Δ*pdhS2* Δ*dgcB* (ΔAtu1888 ΔAtu1691)	This study
A. tumefaciens	C58-JEH132	Δ*pdhS2* Δ*dgcC* (ΔAtu1888 ΔAtu2179)	This study
A. tumefaciens	C58-JEH146	Δ*pdhS2* Δ*crdS* Δ*chvAB* Δ*cel* Δ*upp* Δ*exoA* (ΔAtu1888 ΔAtu3055-3057 ΔAtu2728-2730 ΔAtu3302-8187 ΔAtu1235-1240 ΔAtu4053)	This study
A. tumefaciens	C58-JEH147	Δ*pdhS2* Δ*upp* (ΔAtu1888 ΔAtu1235-1240)	This study

bioRxiv preprint doi: https://doi.org/10.1101/148429; this version posted March 30, 2018. The copyright holder for this preprint (which was not certified by peer review) is the author/funder, who has granted bioRxiv a license to display the preprint in perpetuity. It is made available under aCC-BY-NC-ND 4.0 International license.

A. tumefaciens	C58-JEH148	Δ*pdhS2* Δ*cel* (ΔAtu1888 ΔAtu3302-8187)	This study
A. tumefaciens	C58-JEH149	Δ*pdhS2* Δ*crdS* (ΔAtu1888 ΔAtu3055-3057)	This study
A. tumefaciens	C58-JEH150	Δ*pdhS2* Δ*chvAB* (ΔAtu1888 ΔAtu2728-Atu2730)	This study
A. tumefaciens	C58-JEH151	Δ*pdhS2* Δ*exoA* (ΔAtu1888 ΔAtu4053)	This study
A. tumefaciens	C58-JEH153	Δ*divK* Δ*pdhS2* (ΔAtu1296 ΔAtu1888)	This study
A. tumefaciens	C58-JW7	Δ*divK* (ΔAtu1296)	(2)
A. tumefaciens	C58-JW8	Δ*pleD* (ΔAtu1297)	(2)
A. tumefaciens	C58-JX100	Δ*crdS* (ΔAtu3055-3057)	(3)
A. tumefaciens	C58-JX101	Δ*chvAB* (ΔAtu2728-2730)	(3)
A. tumefaciens	C58-JX102	Δ*cel* (ΔAtu3302-8187)	(3)
A. tumefaciens	C58-JX111	Δ*crdS* Δ*chvAB* Δ*cel* Δ*upp* Δ*exoA* (ΔAtu3055-3057 ΔAtu2728-2730 ΔAtu3302-8187 ΔAtu1235-1240 ΔAtu4053; “EPS$^-$”)	(3)
A. tumefaciens	C58-JX125	Δ*dgcA* (ΔAtu1257)	(4)
A. tumefaciens	C58-JX187	Δ*dgcB* (ΔAtu1691)	(4)

bioRxiv preprint doi: https://doi.org/10.1101/148429; this version posted March 30, 2018. The copyright holder for this preprint (which was not certified by peer review) is the author/funder, who has granted bioRxiv a license to display the preprint in perpetuity. It is made available under aCC-BY-NC-ND 4.0 International license.

A. tumefaciens	C58-MLL2 A	Δ*exoA* (ΔAtu4053)	(5)
A. tumefaciens	C58-PMM26	Δ*upp* (ΔAtu1235-1240)	(3)
A. tumefaciens	C58-YW010	Δ*dgcC* (ΔAtu2179)	(4)
E. coli	S17-1 λ*pir*	RK2 *tra* regulon, *pir*, host for *pir*-dependent plasmids	(6)
E. coli	TOP10 F'	F'{*lac*I^{q} Tn*10* (Tet^{R})} *mcr*A Δ(*mrr-hsd*RMS-*mcr*BC) Φ80*lacZ*ΔM15 Δ*lac*X74 *rec*A1 *ara*D139 Δ(*ara-leu*)7697 *gal*U *rps*L *end*A1 *nup*G	Thermo Fisher Scientific

bioRxiv preprint doi: https://doi.org/10.1101/148429; this version posted March 30, 2018. The copyright holder for this preprint (which was not certified by peer review) is the author/funder, who has granted bioRxiv a license to display the preprint in perpetuity. It is made available under aCC-BY-NC-ND 4.0 International license.

Table S2. Plasmids used in this study

Plasmid name	Relevant characteristics	Source
pGEM-T Easy	PCR cloning vector; Amp^R	Promega
p*lacZ*/290	Broad host range plasmid carrying promoterless *lacZ* for transcriptional fusions; Tet^R	(7)
pNPTS138	ColE1 origin; *sacB*; Km^R	gift of M. Alley
pRA301	Broad host range plasmid carrying promoterless *lacZ* for translational fusions; $Spec^R$	(8)
pSRKGm	Broad host range vector containing P_{lac}; $lacI^q$; $lacZ\alpha^+$; Gm^R	(9)
p*ctrA*290	p*lacZ*/290 derivative with *C. crescentus ctrA* promoter	(10)
pDC001	pGEM-T Easy with full-length $pdhS2^{(CA811\text{-}812GC, A823G)}$ ($PdhS2^{His271A,Thr275Ala}$ mutant)	This study

bioRxiv preprint doi: https://doi.org/10.1101/148429; this version posted March 30, 2018. The copyright holder for this preprint (which was not certified by peer review) is the author/funder, who has granted bioRxiv a license to display the preprint in perpetuity. It is made available under aCC-BY-NC-ND 4.0 International license.

pDC002	pSRKGm with full-length *pdhS2*$^{(CA811\text{-}812GC,\ A823G)}$ (PdhS2^{His271A,Thr275Ala} mutant)	This study
pGZ22	p*lacZ*/290 derivative with *C. crescentus ccrM* promoter	(11)
pJEH010	pSRKGm with full-length wild-type *cckA*	(2)
pJEH021	pGEM-T Easy with full-length *pdhS2*	(2)
pJEH026	pSRKGm with full-length *pdhS2*	(2)
pJEH030	pSRKGm with full-length Y674D *cckA* allele	(2)
pJEH040	pNPTS138 derivative with *pdhS2* SOE deletion fragment	(2)
pJEH052	pGEM-T Easy with *pdhS2* lacking a stop codon	This study
pJEH053	pGEM-T Easy with *gfpmut3*	This study

bioRxiv preprint doi: https://doi.org/10.1101/148429; this version posted March 30, 2018. The copyright holder for this preprint (which was not certified by peer review) is the author/funder, who has granted bioRxiv a license to display the preprint in perpetuity. It is made available under aCC-BY-NC-ND 4.0 International license.

pJEH054	pGEM-T Easy with *divJ* lacking a stop codon	This study
pJEH060	pSRKGm with a *pdhS2*::*gfpmut3* translational fusion	This study
pJEH078	pSRKGm with a *divJ*::*gfpmut3* translational fusion	This study
pJEH091	pGEM-T Easy with full-length *pdhS2*$^{(CA811-812GC)}$ (PdhS2^{His271Ala} mutant)	This study
pJEH092	pSRKGm with full-length *pdhS2*$^{(CA811-812GC)}$ (PdhS2^{His271Ala} mutant)	This study
pJEH099	pGEM-T Easy with full-length *pdhS2*$^{(A823G)}$ (PdhS2^{Thr275Ala} mutant)	This study
pJEH102	pSRKGm with full-length *pdhS2*$^{(A823G)}$ (PdhS2^{Thr275Ala} mutant)	This study
pJEH113	pGEM-T Easy with *A. tumefaciens ccrM* promoter	This study

bioRxiv preprint doi: https://doi.org/10.1101/148429; this version posted March 30, 2018. The copyright holder for this preprint (which was not certified by peer review) is the author/funder, who has granted bioRxiv a license to display the preprint in perpetuity. It is made available under aCC-BY-NC-ND 4.0 International license.

pJEH115	pGEM-T Easy with *A. tumefaciens ctrA* promoter	This study
pJEH119	pGEM-T Easy with *A. tumefaciens pdhS1* promoter	This study
pJEH121	pRA301 with *A. tumefaciens ccrM* promoter	This study
pJEH122	pRA301 with *A. tumefaciens ctrA* promoter	This study
pJEH124	pRA301 with *A. tumefaciens pdhS1* promoter	This study
pJEH133	pRA301 with mutated *A. tumefaciens dgcB* promoter	This study
pJS70	p*lacZ*/290 derivative with *C. crescentus pilA* promoter	(12)
pJX158	pRA301 with *A. tumefaciens* Atu3318 promoter	(4)

bioRxiv preprint doi: https://doi.org/10.1101/148429; this version posted March 30, 2018. The copyright holder for this preprint (which was not certified by peer review) is the author/funder, who has granted bioRxiv a license to display the preprint in perpetuity. It is made available under aCC-BY-NC-ND 4.0 International license.

pJX162	pRA301 with *A. tumefaciens dgcB* promoter	(4)
pJX520	pSRKGm with full-length *dgcB*	(4)
pJX521	pSRKGm with full-length *dgcB*$^{A767C, A770C}$ (DgcB$^{EE256-257AA}$ mutant)	(4)
pJX802	pNPTS138 derivative with *dgcB* SOE deletion fragment	(4)
pJZ383	pPZP201 derivative with P_{tac}::*gfpmut3*; Spec^{R}	(13)

bioRxiv preprint doi: https://doi.org/10.1101/148429; this version posted March 30, 2018. The copyright holder for this preprint (which was not certified by peer review) is the author/funder, who has granted bioRxiv a license to display the preprint in perpetuity. It is made available under aCC-BY-NC-ND 4.0 International license.

Table S3. Primers used in this study

Primer	Sequence (5' – 3')	Use
JEH65	GAAGAACATATGAGTAAAAGCGTCAGCA	cloning *pdhS2* with NdeI site
JEH85	GATTTCGCGCGATCCCTTCGA	Internal primer for *pdhS2* locus
JEH87	GAGCAGATGCTGGCCGGA	Internal primer for *pdhS2* locus
JEH100	GCTCTGTTGAAGGCGGCCAA	External primer for *pdhS2* locus
JEH113	GCCGGTTTCATGCACACGCA	External primer for *pdhS2* locus
JEH146	GAAGAAGCTAGCGGCGAAAGACCGCCGG	cloning *pdhS2* w/o STOP and with NheI site
JEH147	GAAGAACATATGAGAGAAAAAGCGGTCGCA	cloning *divJ* with NdeI site
JEH148	GAAGAAGCTAGCGGCGATTTTCGCTTTCGCGG	cloning *divJ* w/o STOP and with NheI site
JEH149	GAAGAAGGTACCTTATTTGTATAGTTCATCCATGCCA	cloning *gfpmut3* with KpnI site
JEH150	GAAGAAGCTAGCATGAGTAAAGGAGAAGAACTT	cloning *gfpmut3* with NheI site
JEH245	CGTGCGCAGCTCGgcCGACATGGAAGCG	*pdhS2*$^{CA811-812GC}$ mutagenesis
JEH246	CGCTTCCATGTCGgcCGAGCTGCGCACG	*pdhS2*$^{CA811-812GC}$ mutagenesis
JEH261	CGCACGAGCTGCGCgCGCCGCTCAACGC	*pdhS2*^{A823G} mutagenesis
JEH262	GCGTTGAGCGGCGcGCGCAGCTCGTGCG	*pdhS2*^{A823G} mutagenesis
JEH282	GGTACCTGCCAGAATCGTTGCT	cloning *ccrM* promoter region, +222 bp to -9 bp from translational start, with KpnI site
JEH284	AAGCTTTGCTGCCATTGGTACT	cloning *ccrM* promoter region, +222 bp to -9 bp from translational start, with HindIII site
JEH285	GGTACCTTAACCTTTCGTTTACGGGCA	cloning *ctrA* promoter region, +328 bp to -9 bp from translational start, with KpnI site
JEH287	CTGCAGAACCCGCATAATTATCCCCTTT	cloning *ctrA* promoter region, +328 bp to -9 bp from

bioRxiv preprint doi: https://doi.org/10.1101/148429; this version posted March 30, 2018. The copyright holder for this preprint (which was not certified by peer review) is the author/funder, who has granted bioRxiv a license to display the preprint in perpetuity. It is made available under aCC-BY-NC-ND 4.0 International license.

		translational start, with PstI site
JEH291	GGTACCATTTGCAAGTGCCTCTT	cloning *pdhS1* promoter region, +264 bp to -9 bp from translational start, with KpnI site
JEH293	AAGCTTGGCGGGCATGTCGAAA	cloning *pdhS1* promoter region, +264 bp to -9 bp from translational start, with HindIII site
USP073	GTTCCCTGAAACTTATTTTTCGTCTATTTTTATCTTATAATTTTGATAATCATCAGTAATTTTCATTTTGTAGGATTTCC	site-directed mutagenesis of CtrA binding site in *dgcB* promoter
USP074	GGAAATCCTACAAAATGAAAATTACTGATGATTATCAAAATTATAAGATAAAAATAGACGAAAAATAAGTTTCAGGGAAC	site-directed mutagenesis of CtrA binding site in *dgcB* promoter

bioRxiv preprint doi: https://doi.org/10.1101/148429; this version posted March 30, 2018. The copyright holder for this preprint (which was not certified by peer review) is the author/funder, who has granted bioRxiv a license to display the preprint in perpetuity. It is made available under aCC-BY-NC-ND 4.0 International license.

REFERENCES

1. **Heindl JE, Crosby D, Brar S, Merenich D, Buechlein AM, Bruger EL, Waters CM, Fuqua C.** 2017. Reciprocal control of motility and biofilm formation by the PdhS2 two-component sensor kinase of Agrobacterium tumefaciens. bioRxiv.
2. **Kim J, Heindl JE, Fuqua C.** 2013. Coordination of division and development influences complex multicellular behavior in Agrobacterium tumefaciens. PLoS One **8:**e56682.
3. **Gao R, Stock AM.** 2017. Quantitative Kinetic Analyses of Shutting Off a Two-Component System. MBio **8**.
4. **Xu J, Kim J, Koestler BJ, Choi JH, Waters CM, Fuqua C.** 2013. Genetic analysis of Agrobacterium tumefaciens unipolar polysaccharide production reveals complex integrated control of the motile-to-sessile switch. Mol Microbiol **89:**929-948.
5. **Grangeon R, Zupan J, Jeon Y, Zambryski PC.** 2017. Loss of PopZ At activity in Agrobacterium tumefaciens by Deletion or Depletion Leads to Multiple Growth Poles, Minicells, and Growth Defects. MBio **8**.
6. **Simon R, Priefer U, Puhler A.** 1983. A broad host range mobilization system for *in vivo* genetic engineering: transposon mutagenesis in gram negative bacteria. Bio/Technology (Nature Publishing Company) **Nov.:**784-791.
7. **Gober JW, Shapiro L.** 1992. A developmentally regulated *Caulobacter* flagellar promoter is activated by 3' enhancer and IHF binding elements. Mol Biol Cell **3:**913-926.
8. **Akakura R, Winans SC.** 2002. Constitutive mutations of the OccR regulatory protein affect DNA bending in response to metabolites released from plant tumors. J Biol Chem **277:**5866-5874.
9. **Khan SR, Gaines J, Roop RM, 2nd, Farrand SK.** 2008. Broad-host-range expression vectors with tightly regulated promoters and their use to examine the influence of TraR and TraM expression on Ti plasmid quorum sensing. Appl Environ Microbiol **74:**5053-5062.
10. **Domian IJ, Reisenauer A, Shapiro L.** 1999. Feedback control of a master bacterial cell-cycle regulator. Proc Natl Acad Sci U S A **96:**6648-6653.
11. **Stephens CM, Zweiger G, Shapiro L.** 1995. Coordinate cell cycle control of a Caulobacter DNA methyltransferase and the flagellar genetic hierarchy. J Bacteriol **177:**1662-1669.
12. **Skerker JM, Shapiro L.** 2000. Identification and cell cycle control of a novel pilus system in Caulobacter crescentus. EMBO J **19:**3223-3234.
13. **Ramey BE, Matthysse AG, Fuqua C.** 2004. The FNR-type transcriptional regulator SinR controls maturation of *Agrobacterium tumefaciens* biofilms. Molecular Microbiology **52:**1495-1511.